Research Square

Preprints are preliminary reports that have not undergone peer review.
They should not be considered conclusive, used to inform clinical practice,
or referenced by the media as validated information.

Can Low-Cost Sensor Networks Improve Analysis of Extreme Pollution Episodes in Delhi During Stubble Burning?

Prafull P. Yadav

prafull.yadav@tropmet.res.in

Indian Institute of Tropical Meteorology

Rajmal Jat

Indian Institute of Tropical Meteorology

Gaurav Govardhan

Indian Institute of Tropical Meteorology

Rajesh Kumar

NSF National Center for Atmospheric Research

Prabir K. Patra

Research Institute for Humanity and Nature

Yutaka Matsumi

Nagoya University

Tomoki Nakayama

Nagasaki University

Sachiko Hayashida

Research Institute for Humanity and Nature

Aditi Rathore

Indian Institute of Tropical Meteorology

Vikram Kadam

Indian Institute of Tropical Meteorology

Chinmay Jena

India Meteorological Department

Sachin D. Ghude

Indian Institute of Tropical Meteorology

Article

Keywords: $PM_{2.5}$ data assimilation, low-cost sensors, crop-residue burning, Indo-Gangetic Plain, 3DVAR

Posted Date: November 3rd, 2026

DOI: https://doi.org/10.21203/rs.3.rs-11388680/v1

License: This work is licensed under a Creative Commons Attribution 4.0 International License.
Read Full License

Additional Declarations: No competing interests reported.

Abstract

Extreme post-monsoon $PM_{2.5}$ episodes across the Indo-Gangetic Plain are often underestimated because fire-emission uncertainties coincide with sparse reference-grade monitoring in crop-residue-burning source regions. We assess whether a low-cost sensor network deployed across source regions can improve atmospheric composition forecasts during November 2024. Twice-daily $PM_{2.5}$ observations from 33 CUPI-G sensors across rural source areas and downwind transport pathways were assimilated into WRF-Chem using 3D-Var. DA-EXP1, using a realistic 10% observation error, reduced mean fractional bias over Haryana from − 116.7% to − 56.8% and correctly predicted the observed Severe AQI category in approximately 95% of Delhi cases and 100% of Punjab and Haryana cases; CNTL predicted no Severe cases at these locations. DA-EXP2, using a 1.5 μg m^{-3} observation error representative of reference-grade monitoring stations, provided further improvements, highlighting the importance of observation-error specification. These results demonstrate the operational value of assimilating source-region low-cost observations into AIRWISE for extreme-pollution forecasting and early warning.

Introduction

Fine particulate matter ($PM_{2.5}$) over the Indo-Gangetic Plain (IGP) reaches its highest levels during the post-monsoon season, when daily mean concentrations over Delhi-NCR frequently exceed the Indian National Ambient Air Quality Standard (NAAQS) by an order of magnitude and hourly values can surpass 1000 μg m^{-3} [1,2]. Exposure to such extreme pollution poses serious health risks and contributes significantly to premature mortality in India[3,4,5]. Accurate short-term (1–3 days) $PM_{2.5}$ forecasts are therefore essential for supporting air-quality management measures, including the Graded Response Action Plan (GRAP) implemented by the Commission for Air Quality Management (CAQM)[6]. Under GRAP, progressively stringent response measures are required as air quality deteriorates. Reliable forecasts can provide advanced warning of impending Very Poor and Severe air-quality episodes, allowing authorities to implement timely measures to reduce public exposure and support coordinated air-quality management.

The seasonal deterioration of air quality is driven by the coincidence of two factors. First, the harvest of kharif rice in October–November followed by widespread crop-residue burning (CRB) across Punjab and Haryana, releasing large quantities of primary $PM_{2.5}$, carbon monoxide and secondary-aerosol precursors into the boundary layer[7,8,9]. Accurately quantifying these emissions remains challenging because fire activity exhibits strong spatial and temporal variability, and recent studies have shown a shift of burning activity from daytime to evening hours[7]. Consequently, polar-orbiting satellite-based fire detection systems may miss a substantial fraction of burning events due to their limited overpass times, cloud and fog contamination, and reduced visibility during severe haze episodes, leading to large uncertainties in fire-emission inventories and model simulations[8,9,10,11,12]. Second, the post-monsoon transition to persistent north-westerly winds, together with falling temperatures, a shallow planetary boundary layer (PBL) and near-absent rainfall, favours the accumulation and transport of these

emissions towards Delhi-NCR[13,14,15]. When intense emissions coincide with stagnant meteorological conditions, the entire IGP can be engulfed in a multi-day haze layer with hourly $PM_{2.5}$ concentrations exceeding 1000 μg m^{-3}[16].

Despite their operational importance, regional Atmospheric Composition Models (ACMs) such as WRF-Chem — coupled meteorology–chemistry models of trace-species emission, transport, transformation and removal systematically underestimate peak haze over this region[5,14,17,18,19]. The underestimation stems from uncertainties in fire-emission inventories (burning fraction and fuel load), missing or under-represented secondary organic aerosol (SOA) formation, biases in boundary-layer dynamics, and coarse horizontal resolution that smears CRB plume gradients[15,19]. To counter these errors, operational systems — including the Air Quality Warning and Integrated Decision Support System for Emissions (AIRWISE), developed by the Indian Institute of Tropical Meteorology, Pune — assimilate observational constraints into the model state, most commonly satellite-retrieved aerosol optical depth (AOD) using variational schemes built on the community Gridpoint Statistical Interpolation (GSI) framework[19,20,21,22,23].

The effectiveness of satellite AOD assimilation decreases during extreme pollution characterized by dense smoke, fog, and low clouds episodes because aerosol retrievals from Moderate Resolution Imaging Spectroradiometer (MODIS), Visible Infrared Imaging Radiometer Suite (VIIRS), and Ocean Colour Monitor (OCM) require clear-sky conditions and are often unavailable under such conditions. During severe post-monsoon events, these limitations lead to missed fire activity, results into underestimated emissions, and so the $PM_{2.5}$ concentrations in model simulations[16,19]. Consequently, satellite-based constraints become least effective when pollution levels are highest. This limitation is particularly evident during the November 2024 episode, when extensive retrieval gaps were observed over Punjab and the northwestern IGP, even in the high-resolution OCM observations (Fig. 3).

The November 2024 episode exposed a key limitation of satellite-constrained emission inventories. Although WRF-Chem simulations suggested that the contribution of crop-residue burning to Delhi-NCR $PM_{2.5}$ declined from 18% in 2022 and 16% in 2023 to only 9% in 2024, consistent with fewer satellite-detected fires, observations from the CUPI-G (Compact and Useful $PM_{2.5}$ Instrument with Gas sensors) network showed persistently high $PM_{2.5}$ levels across rural Punjab[11]. This mismatch indicates that a significant fraction of burning activity was likely missed by satellites, particularly during evening hours and under foggy or cloudy conditions, resulting in underestimated fire emissions and $PM_{2.5}$ concentrations[11]. They attributed this paradox to a shift in burning from the early afternoon to the evening, after the Terra MODIS (~ 10:30 IST) and Aqua MODIS and Suomi-NPP/VIIRS (~ 13:30 IST) overpasses. As a result, inventories based mainly on daytime polar-orbiting fire detections may substantially underestimate evening emissions. These emissions are then released into a shallow and stable evening boundary layer, where pollutants accumulate strongly through the night. Thus, the November 2024 episode highlights two related limitations of satellite-based constraints: missed evening fire detections and missing clear-sky AOD retrievals during fog and haze. Both limitations point to the

need for continuous surface-based observations that can directly capture near-surface $PM_{2.5}$ build-up after satellite overpass and during nighttime hours.

A complementary, and increasingly mature, source of such a constraint is the dense in-situ low-cost sensor network. Low-cost sensors have driven a paradigm shift in air-quality monitoring, supplementing sparse reference-grade networks with high-density, real-time observations that resolve pollution gradients and hotspots which regulatory monitoring stations cannot[1,24,25,26,27]- this densification is especially valuable in India, where the reference network is limited to urban centres and unevenly distributed[28]. Deployed under the Aakash project (Research Institute for Humanity and Nature), the CUPI-G pairs a palm-sized optical $PM_{2.5}$ sensor developed by Nagoya University and Panasonic with electrochemical gas sensors, costs roughly 1/100th of a reference-grade analyser, runs autonomously on solar power or a rechargeable battery, and reports in near real time[31,16,30].Prior work has exploited this network only indirectly: Kajino et al. (2024)[31] used CUPI-G observations to optimize CRB emissions in NHM-Chem (Non-Hydrostatic Model) for November 2022, inferring a mean surface CRB contribution of 30%–34% rising to 50%–56% during downwind plume transport from the Punjab source region to Delhi-NCR, while Singh et al. (2023)[16] and Mangaraj et al. (2025)[15] characterized the 2022 and 2023 seasons. These studies adjusted emissions offline, but none has assimilated the low-cost network directly into the model state with the objective of improving air quality forecasts.

In this study, we test the central hypothesis that assimilating widespread low-cost CUPI-G surface $PM_{2.5}$ observations over northwestern India directly into the WRF-Chem state can recover an extreme pollution episode that the model otherwise fails to capture, particularly when conventional satellite AOD constraints are unavailable. We focus on the 10–21 November 2024 episode, a peak biomass-burning period during which surface $PM_{2.5}$ exceeded 1000 μg m^{-3} and the AQI remained in the Severe category for more than five consecutive days. CUPI-G observations are assimilated twice daily at 00 UTC and 15 UTC. These two cycles are treated as discrete analysis times rather than long averaging windows. The 00 UTC cycle represents the early-morning condition after nocturnal pollutant accumulation under a shallow boundary layer, whereas the 15 UTC cycle represents the evening/post-overpass period, when crop-residue burning emissions are likely to be missed by daytime polar-orbiting satellites and pollutants begin to accumulate within the stable evening boundary layer. We design three experiments: a control simulation without assimilation and two assimilation experiments that differ only in the prescribed observation error, to examine how strongly the model state should be constrained by low-cost $PM_{2.5}$ observations. To our knowledge, this is the first demonstration over India of assimilating a dense low-cost $PM_{2.5}$ sensor network into a regional atmospheric composition model to improve the analysis of an extreme crop-residue-burning pollution episode across Punjab, Haryana.

Results

The November 2024 episode and the rationale for assimilating the low-cost sensor network

The November 2024 post-monsoon period over northwestern India produced an extreme particulate-pollution episode, which forms the basis of the assimilation experiments in this study. Figure 1 shows hourly surface $PM_{2.5}$ concentrations from the CUPI-G network during 10–21 November 2024, grouped into five representative regions: Delhi, Punjab, Haryana, Meerut, and Indian Institute of Technology Roorkee (IIT- Roorkee). The period coincides with peak crop-residue-burning activity over Punjab and Haryana, leading to persistently high regional $PM_{2.5}$ levels. Superimposed on this elevated background are sharp hourly peaks, indicating the passage of intense pollution plumes across the sensor locations.

The maximum hourly $PM_{2.5}$ values, marked by red stars in each panel, reached 1388 μg m^{-3} in Delhi and 1239 μg m^{-3} in Meerut during 17–18 November 1032 μg m^{-3} in Punjab on 12 November, 909 μg m^{-3} in Haryana on 17 November, and 558 μg m^{-3} at IIT-Roorkee on 13 November. These concentrations were several times higher than the Severe AQI threshold of 250 μg m^{-3}. Importantly, the episode was not limited to short-lived peaks; $PM_{2.5}$ remained above the Severe threshold for several consecutive days in Delhi, Haryana, and Meerut. The earlier peak over Punjab, followed by later maxima over Delhi, Haryana, and Meerut, is consistent with the build-up and downwind transport of pollution from the northwestern crop-residue-burning source region toward Delhi-NCR. The sustained severe conditions during 16–18 November make this period a critical test case for evaluating whether data assimilation of low cost CUPI-G observations can improve the model representation of extreme $PM_{2.5}$ episodes.

The spatial structure and transport of $PM_{2.5}$ during this episode are captured by the model. Figure 2 shows the mean surface $PM_{2.5}$ concentration and 10 m wind field simulated by WRF-Chem during 10–21 November 2024, based on the DA-EXP2 simulation. The low-level flow across the domain is north-westerly, carrying air from the Punjab and Haryana source regions down to the IGP toward Delhi-NCR and the areas to the southeast, where the highest mean concentrations (exceeding 150–200 μg m^{-3}) are simulated. The mechanism is straightforward: during the dry post-monsoon period, $PM_{2.5}$ can remain in the atmosphere for several days, much longer than the time required for winds to transport air masses across the study domain. The particles therefore behave largely as transported tracers in the atmosphere. Once emitted by burning in the northwest, they are carried downwind by the prevailing north-westerly flow rather than being removed or dispersed locally. In plain terms, the wind blows from the burning fields in Punjab and Haryana toward Delhi, and the smoke travels with it — which is why the surface concentration is highest along and at the downwind end of that path. This is the same physical link that explains the sequence of concentration peaks in Fig. 1: the Punjab peak appears first because that is where the emissions originate, and the Delhi peak follows a few days later as the polluted air arrives. The persistence of this north-westerly regime over the whole episode is what makes the pollution regionally coherent rather than confined to any single city.

Figure 2. Mean surface $PM_{2.5}$ concentration (μg m^{-3}; shaded) overlaid with 10 m wind vectors, averaged over 10–21 November 2024, from the DA-EXP2 assimilation experiment over the analysis domain. The north-westerly low-level flow advects pollution from the Punjab and Haryana CRB source regions toward Delhi-NCR and the downwind areas to the southeast.

This episode was difficult to constrain observationally because satellite AOD retrievals, which are conventionally assimilated to correct the modelled aerosol field, were frequently unavailable over the affected region. Figure 3 shows the daily OCM AOD distribution during 10–21 November 2024, with extensive white areas over Punjab, Haryana, and the central Indo-Gangetic Plain indicating missing retrievals on several days of the episode. These gaps reflect dense fog, haze, and low-cloud conditions that prevented reliable observations of the aerosol column. Complementary evidence is provided in Figure S1, which shows the INSAT-3DR (Indian National Satellite System–3DR) fog/low-cloud product and indicates widespread fog and low cloud over the Punjab–Haryana–Delhi corridor during key days of the episode.

The same conditions that limit AOD retrievals can also reduce satellite detection of active fires. Consequently, both the biomass-burning emissions used to drive the model and the satellite AOD observations used to constrain the aerosol field were degraded during this period[11,19]. This simultaneous limitation of emission estimates and satellite aerosol observations restricts the ability of the model to represent the episode using satellite information alone and motivates the use of continuous surface-based observations from the CUPI-G network.

Chemical data assimilation has been widely used to improve the initial chemical conditions and short-range WRF-Chem forecasts over India, including $PM_{2.5}$ prediction during the paddy-residue-burning season over Delhi[20], the operational AIRWISE $PM_{2.5}$ forecasting system based on 3D-Var assimilation[21], assimilation of VIIRS AOD retrievals[22], and surface $PM_{2.5}$ observations from CPCB network, mainly located in Urban centers[18]. However, these applications rely mainly on satellite AOD observations, which provide limited constraints during the present episode because of the retrieval gaps described above. In addition, the CPCB monitoring network, although highly accurate, has no coverage over rural Punjab, the major crop-residue-burning source region and the upwind part of the transport pathway.

The CUPI-G network addresses this observational gap by providing dense, continuous, in-situ $PM_{2.5}$ measurements across the source region covering rural biomass burning affected areas in Punjab and Haryana and the downwind transport corridor, independent of cloud cover and satellite overpass timing. Assimilating these observations can therefore constrain the evolving pollution plume in regions where satellite AOD and regulatory observations are insufficient. The following sections evaluate the impact of this assimilation and its sensitivity to the assumed observation error in DA-EXP1 and DA-EXP2.

Effect of assimilation on the simulated $PM_{2.5}$

Figure 4 compares the hourly observed $PM_{2.5}$ (OBS) with the control simulation (CNTL) and the two assimilation experiments (DA-EXP1 and DA-EXP2) over 10–21 November 2024 for the five regions: Punjab, Haryana, IIT-Roorkee, Delhi and Meerut. The control simulation captures the broad temporal evolution of the episode but substantially underestimates $PM_{2.5}$ concentrations across all regions. CNTL remains relatively low and exhibits limited day-to-day variability, with concentrations generally between

50 and 150 μg m^{-3}. It fails to represent the magnitude of the observed pollution peaks: during the Delhi and Meerut maxima of 17–18 November, when observed $PM_{2.5}$ approached 1200–1400 μg m^{-3} (Fig. 4d, e), CNTL remained below 200 μg m^{-3}. Similarly, during the Punjab peak on 12 November (Fig. 4a), CNTL underestimated the observed concentration by nearly an order of magnitude. This persistent low bias is consistent with the underestimation of biomass-burning emissions in the control simulation, as a substantial fraction of fire activity was not captured by satellite-based fire products during the episode.

Both assimilation experiments improve the representation of the magnitude and temporal evolution of the major $PM_{2.5}$ peaks across the five regions. The improvement is most evident during periods when CNTL shows the largest negative bias, indicating that the assimilation draws the model state closer to the surface observations due to surface $PM_{2.5}$ assimilation from CUPI-G network when the satellite-constrained observations are sparsely available. DA-EXP2 captures the sharp temporal variability more closely over Delhi, Haryana, and Meerut (panels b, d, and e), with analysed concentrations approaching the observed peak values, whereas CNTL substantially underestimates the magnitude of these peaks.

The two assimilation experiments exhibit broadly similar temporal variations, although their amplitudes differ across regions and stages of the episode. DA-EXP2 generally yields higher analysed $PM_{2.5}$ concentrations than DA-EXP1 during periods of elevated pollution, highlighting the positive feedback of improvement in measurement error of low-cost sensors. The separation between the two experiments is evident over Punjab during 12–16 November, around 15 November at IIT-Roorkee, and most prominently over Haryana, Delhi, and Meerut during 15–19 November. This divergence is a direct consequence of the observation-error prescription adopted in each experiment. DA-EXP2, which applies the fixed regulatory error of 1.5 μg m^{-3}, places substantially greater trust in the CUPI-G observations relative to the model background and therefore pulls the analysed concentrations more strongly toward the observed values, recovering the highest peak concentrations of the two experiments. DA-EXP1, which instead assigns an observation error of approximately 10% of the observed value — reaching nearly 100 μg m^{-3} at peak pollution levels retains considerably more influence from the deficient model background during the most polluted hours, resulting in lower recovered concentrations. When observed $PM_{2.5}$ concentrations were lower, the difference between the prescribed observation errors in DA-EXP1 and DA-EXP2 was smaller, and the two analyses showed similar $PM_{2.5}$ concentrations. During periods of very high $PM_{2.5}$, the observation-error specification had a stronger influence on the analysis because the model background remained far below the observations. Thus, the magnitude of the analysis increment depended strongly on the prescribed observation error and the resulting relative weighting of the CUPI-G observations and model background.

To examine where the differences between the two experiments are spatially concentrated, Fig. 5 presents the episode-mean difference in surface $PM_{2.5}$ between DA-EXP2 and DA-EXP1, averaged over the full simulation period of 10–21 November 2024. The difference field is positive across the entire domain, confirming that DA-EXP2 systematically recovers higher surface $PM_{2.5}$ than DA-EXP1 throughout the episode, with the largest enhancements concentrated over the Delhi-NCR and its immediate surroundings. Here, the episode-mean difference exceeds 100 μg m^{-3}, coinciding with the

region of most intense observed pollution during the episode. The maximum enhancement, reaching approximately 80–100 μg m^{-3}, is centred over the Delhi-NCR region near 77°E and 28.5–29°N. Smaller but distinct positive differences, generally ranging from about 20 to 60 μg m^{-3}, are distributed across Punjab and Haryana along the source-to-receptor transport pathway. This pattern indicates that the influence of the observation-error specification is strongest in regions affected by the most intense pollution. DA-EXP2, placing greater trust in the CUPI-G observations, produces substantially larger corrections to the background state than DA-EXP1 in this region. A secondary maximum is also evident over the Punjab cluster, consistent with the intense fire-driven pollution peak observed around 12 November, reinforcing that the spatial pattern of inter-experiment differences closely tracks the pollution episode itself rather than simply reflecting the spatial distribution of the observation network. Overall, these two experiments with two different error characteristics suggest that improvements in the measurement errors of low-cost sensors can substantially improve the model predictions closer to reality and increase the reliability of low-cost sensors in modelling studies.

Statistical evaluation of the assimilation experiments

The spatial and temporal improvements described in above section are further supported quantitatively by the error statistics presented in Table 1, which reports the root mean square error (RMSE), mean fractional bias (MFB), normalised mean bias (NMB), and index of agreement (IOA) for CNTL, DA-EXP1, and DA-EXP2 across all five regions over the simulation period of 10–21 November 2024.

The control simulation shows consistent negative bias across all regions, confirming the underestimation of surface $PM_{2.5}$ evident in the time-series analysis. MFB ranges from − 68.8% over Delhi to − 126.2% over Punjab, while NMB ranges from − 59.9% to − 81.8%, indicating that the model background remains far below the observed $PM_{2.5}$ concentrations throughout the episode. This bias is especially important over Punjab, where the strongest negative MFB indicates that the model does not adequately represent the fire-driven pollution loading near the source region. The largest RMSE values occur over Punjab (417.9 μg m^{-3}) and Delhi (390.3 μg m^{-3}), showing that errors in the background field affect both the source region and the downwind urban receptor region. The low IOA values across all regions (0.40–0.46) further indicate limited agreement between the simulated and observed temporal variability. Together, these results show that the control simulation provides an insufficient chemical background for representing the magnitude and regional evolution of this severe $PM_{2.5}$ episode.

Table 1
Statistical evaluation of the control simulation (CNTL) and the two assimilation experiments (DA-EXP1 and DA-EXP2) against hourly observed surface $PM_{2.5}$ concentrations over the simulation period 10–21 November 2024.

Experiment	Region	RMSE (ug m^{-3})	MFB (%)	NMB (%)	IOA
CNTL	Delhi	390.3	-68.8	-59.90	0.46
	Punjab	417.9	-126.2	-81.8	0.43
	Haryana	336.3	-116.7	-78.2	0.44
	Meerut	329.4	-75.8	-67.2	0.44
	IIT Roorkee	174.9	-111.8	-74.6	0.4
DA-EXP1	Delhi	317.2	-20.2	-32.74	0.48
	Punjab	356	-90.24	-66.19	0.47
	Haryana	251.7	-56.8	-49.81	0.52
	Meerut	313.9	-55.1	-56.75	0.42
	IIT Roorkee	115.26	-46.7	-40.48	0.52
DA-EXP2	Delhi	320.01	-13.86	-19.66	0.56
	Punjab	313.77	-66.09	-53.49	0.5
	Haryana	189.25	-27.72	-29.98	0.64
	Meerut	273.97	-18.71	-33.81	0.45
	IIT Roorkee	115.63	-35.4	-32.71	0.49

Assimilation of CUPI-G observations in DA-EXP1 improves all four-evaluation metrics across the five regions. RMSE decreases at every location relative to CNTL, with the largest reductions over Haryana, from 336.3 μg m^{-3} to 251.7 μg m^{-3}, and Delhi, from 390.3 μg m^{-3} to 317.2 μg m^{-3}. The magnitudes of the negative MFB and NMB values are reduced by approximately half across most regions, indicating a reduction in the systematic underestimation of $PM_{2.5}$. These improvements indicate that the assimilation corrects the aerosol field where the model background is affected by underestimated crop-residue-burning emissions. IOA also increases across all regions, reaching 0.52 over Haryana and IIT-Roorkee. However, the smaller IOA improvements over Delhi and Meerut indicate limited agreement with the observed temporal evolution, as the assimilated simulations remain below the highest observed $PM_{2.5}$ concentrations during 17–18 November.

Relative to DA-EXP1, DA-EXP2 provides further enhancement across most regions, consistent with the greater observational weight associated with its smaller prescribed error. Over Haryana, RMSE decreases from 251.7 to 189.3 μg m^{-3}, while MFB changes from − 56.8% to − 27.7%, showing that DA-

EXP2 reduces both the overall error and the negative bias relative to DA-EXP1. The IOA also increases from 0.52 to 0.64, indicating closer correspondence with the observed temporal pattern. This is the highest IOA obtained among all regions and experiments in this study. This is physically interpretable in the context of the episode: Haryana, represented by 11 observation sites distributed across a region lying directly downwind of the Punjab fire cluster experienced sustained pollution with a continuous spatial distribution across the source region maintaining elevated $PM_{2.5}$ concentrations throughout the episode and providing dense observational coverage. Because DA-EXP2 assigns a smaller observation error to these measurements, they exert a stronger influence on the analysis than in DA-EXP1. Over Punjab, where 16 CUPI-G sites provide the densest regional sampling within the network, DA-EXP2 yields lower RMSE (313.8 μg m^{-3} versus 356.0 μg m^{-3}) and a less negative NMB (− 53.5% versus − 66.2%) than DA-EXP1. However, both experiments retain large negative MFB values (− 90.2% in DA-EXP1 and − 66.1% in DA-EXP2), indicating continued underestimation during the intense fire-driven peaks of 11–13 November. The remaining model bias after applying data assimilation indicates that, despite the stronger observational influence in DA-EXP2, the severely underestimated background emissions limit the ability of the analysis to represent the highest $PM_{2.5}$ concentrations over Punjab.

Over Delhi, represented by three observation sites but recording the most extreme $PM_{2.5}$ concentrations of the entire episode, DA-EXP2 achieves a notably reduced NMB of − 19.7% compared to − 32.7% in DA-EXP1, and the IOA improves from 0.48 to 0.56. Over Delhi, RMSE remains high in both assimilation experiments: it was 317.2 μg m^{-3} in DA-EXP1 and 320.0 μg m^{-3} in DA-EXP2. This is mainly associated with the sharp $PM_{2.5}$ peaks during 17–18 November, when observed concentrations exceeded 1200 μg m^{-3} and were not fully captured by either experiment. The exceptional pollution loading over Delhi during this period is not solely attributable to the fire emissions from Punjab and Haryana but is further influenced by local emissions within Delhi and the unique meteorological and topographic setting of the region. Delhi lies at the confluence of the IGP transport corridor and the foothills of the Aravalli range, and during post-monsoon months the combination of shallow nocturnal boundary layers, weak synoptic ventilation, and calm near-surface winds suppresses the vertical and horizontal dispersal of pollutants, promoting the rapid accumulation of both locally emitted and long-range transported aerosols within a shallow mixing volume[32,33,34,35,36,37]. These conditions favour the occurrence of extreme pollution episodes in Delhi when fire-related aerosol transport from the northwest coincides with stagnant meteorological conditions, as observed during 17–18 November 2024, and they represent a source of model error that the assimilation alone cannot fully correct in the absence of accurate boundary layer dynamics. Additionally, the MOZART-GOCART chemistry used in the forecast is a bulk aerosol scheme and missing the Secondary Organic Aerosol (SOA), Ammonium, Nitrate and Chloride aerosol chemistry. At Meerut, the single observation site in Uttar Pradesh, DA-EXP2 achieves a substantially reduced MFB of − 18.7% relative to − 55.1% in DA-EXP1, representing the largest reduction in fractional bias between the two experiments across any region, consistent with the pronounced spatial difference identified over the Delhi NCR and its eastern surroundings in Fig. 5. At IIT-Roorkee, situated at the Himalayan foothills in Uttarakhand at the northern periphery of the IGP pollution corridor, both assimilation experiments perform comparably with nearly identical RMSE values of approximately 115 μg m^{-3}, suggesting that the

marginal benefit of the tighter observation error in DA-EXP2 is limited at locations where the pollution loading is more moderate and the model background is less severely deficient.

Overall, the statistical evaluation confirms that the assimilation of CUPI-G observations produces consistent improvement over the control simulation across all regions and metrics, with the magnitude of improvement scaling with the intensity of the pollution episode and the density of the observation network. The persistent negative biases in DA-EXP2 indicate that, although the assimilation corrects aerosol concentrations at each analysis time, it does not modify the prescribed fire emissions. The model therefore continues to use underestimated fire emissions between assimilation cycles, which can cause $PM_{2.5}$ concentrations to again fall below the observations during the subsequent forecast period. Remaining errors in boundary-layer evolution, regional transport, limitations in forecast chemistry and other model processes may further contribute to this underestimation during the most severe pollution conditions.

Assessment of AQI category agreement between Model and Observations.

While the statistical metrics quantify the magnitude of error in the simulated $PM_{2.5}$ concentrations, they do not directly address the operational utility of the analysis — which, from the perspective of both public communication and policy intervention, lies in the AQI category analysis. This distinction is particularly consequential in the context of the November 2024 IGP episode, where the GRAP interventions enforced by the CAQM are triggered by AQI categories derived from raw $PM_{2.5}$ concentration [21,6]. Following CPCB AQI methodology, the AQI's are estimated using the hourly CUPI-G $PM_{2.5}$ observations and the corresponding model analysis fields for the purpose of categorical evaluation. AQI category match percentages (Eq. 2) were then estimated, which provides a useful diagnostic of whether the assimilation system assigns the observed pollution episode to the correct AQI category at sub-daily timescales. For example, when observed conditions fall within the Very Poor or Severe AQI categories, a low category-match percentage indicates that the model assigns these episodes to lower AQI categories. Such misclassification underestimates the associated air-quality risk and can limit the usefulness of the system for timely implementation of the corresponding GRAP measures.

Figure 6 presents the AQI category match percentage for all five regions for CNTL, DA-EXP1, and DA-EXP2. The results reveal a consistent and physically coherent pattern across all regions: the control simulation fails almost entirely to reproduce the observed AQI categories during the most severe pollution conditions, both assimilation experiments substantially recover the correct category, and DA-EXP2 outperforms DA-EXP1 across the higher AQI classes at most locations — a hierarchy that is directly consistent with the concentration-level improvements in simulated $PM_{2.5}$ and statistical performance..

The categorical failure of CNTL is most apparent in the Very Poor and Severe categories, which dominated the observed AQI during the core of the episode. Over Delhi, CNTL achieves a correct category match of only approximately 20% for Very Poor hours and near zero for Severe hours, which is a

direct consequence of the systematic $PM_{2.5}$ underestimation that causes the model to place the episode in lower AQI classes even when observed concentrations exceeded 500–1000 μg m^{-3}. Over Punjab and Haryana, CNTL achieves virtually no correct matches in either category despite these conditions prevailing for extended periods during 11–13 and 17–19 November, confirming that without assimilation the analysis system provides no reliable identification of the most hazardous air quality conditions of the episode.

The assimilation of CUPI-G observations substantially corrects this categorical misclassification across all regions. Over Delhi, DA-EXP2 achieves correct match rates of approximately 70% for Very Poor category, compared to 47% in DA-EXP1, demonstrating that the tighter observation-error prescription in DA-EXP2 improves not only the continuous concentration metrics but also the categorical representation of the elevated AQI conditions. For the severe AQI category, both DA-EXP1 and DA-EXP2 achieved nearly 90% correct match rates in Delhi. Over Haryana, both experiments achieve near-perfect match rates for the Severe category, though DA-EXP2 substantially outperforms DA-EXP1 for Very Poor hours with approximately 58% against 32%, consistent with the stronger statistical improvements over this region. Over Punjab, DA-EXP2 achieves close to 100% match for the Severe category while DA-EXP1 records near-zero match rates for Very Poor — a distinction with direct implications for the categorical identification of the most intense fire-driven pollution peaks. At Meerut, DA-EXP2 achieves approximately 80% match for Severe hours against a considerably lower rate in DA-EXP1, while both experiments show comparable performance for the Very Poor category, with match rates ranging from 43% to 52%. At IIT-Roorkee, the observed AQI does not reach the Severe category because of the lower pollution levels at this peripheral location. Both experiments show similar match rates, approximately 53%–55% for Very Poor and 30% for Poor, consistent with their similar $PM_{2.5}$ concentrations under conditions below the most extreme pollution levels.

The AQI category match assessment confirms that the assimilation of CUPI-G observations improves not only the quantitative accuracy of the analysed $PM_{2.5}$ but also its categorical utility for air quality management. DA-EXP2 consistently outperforms DA-EXP1 for the Very poor and Severe categories directly relevant to GRAP activation, demonstrating that the observation-error prescription carries consequences for categorical analysis skill upon which regulatory decisions depend. These results highlight the value of integrating low-cost sensor networks such as CUPI-G into operational air quality analysis systems over the IGP, where the accurate categorical representation of extreme post-monsoon pollution episodes remains both a scientific challenge and a public health priority.

Discussion

This study demonstrates, for the first time over India, the effectiveness of assimilating $PM_{2.5}$ concentrations from surface measurements of a dense low-cost $PM_{2.5}$ sensor network into WRF-Chem for analysing an extreme post-monsoon pollution episode over northwestern India. During 10–21 November 2024, hourly $PM_{2.5}$ concentrations exceeded 1000 μg m^{-3} at several locations across Punjab, Haryana and Delhi-NCR, while AQI remained in the Severe category for multiple consecutive days. The

results show that the CUPI-G sensor network provides a valuable surface $PM_{2.5}$ observation and becomes a more useful constraint during conditions when conventional satellite-based aerosol observations are largely unavailable because of dense fog, haze and low cloud. To assess the effectiveness of CUPI-G data, three sets of data assimilation experiments were conducted including CNTL (Without CUPI-G data assimilation), DA-EXP1 (CUPI-G data assimilation with 10% error) and DA-EXP1 (CUPI-G data assimilation with 1.5 μg m^{-3} error).

The control simulation substantially underestimated $PM_{2.5}$ concentrations across the region, with mean fractional biases ranging from − 68.8% over Delhi to − 126.2% over Punjab. Assimilation of CUPI-G observations significantly improved the representation of both the magnitude and temporal evolution of the pollution episode. The improvements were largest during the most intense pollution events and over regions where the control simulation exhibited the greatest underestimation. Among the two experiments, DA-EXP2 consistently outperformed DA-EXP1, achieving an IOA of 0.64 over Haryana and reducing the mean fractional bias over Meerut from − 55.1% to − 18.7%. Nevertheless, DA-EXP1, despite using a realistic 10% low-cost-sensor observation error, substantially improved $PM_{2.5}$ predictions and provided useful forecasts of high-AQI conditions. This shows that the CUPI-G network can provide a meaningful observational constraint for operational assimilation under typical low-cost-sensor uncertainties. The larger corrections obtained in DA-EXP2 indicate that assimilation performance is highly sensitive to the prescribed observation error and suggest that improved characterization of low-cost sensor uncertainties could further reduce model biases during extreme pollution episodes.

The AQI category match further strengthens the assessment and provides the most operationally relevant demonstration of the assimilation benefit. The control simulation fails to identify the Severe and Very Poor categories at most locations, achieving near-zero correct match rates for the categories that would trigger GRAP Stage III and Stage IV interventions. DA-EXP2 recovers correct Severe category match rates of approximately 90% over Delhi and close to 100% over Punjab and Haryana — a transformation from complete categorical failure to near-perfect categorical identification that carries direct consequences for the timeliness and effectiveness of GRAP-based regulatory interventions administered by CAQM. The persistent residual underestimation in both assimilation experiments, particularly over Punjab and Delhi, reflects the fundamental limitation of the strong-constraint variational framework: the deficient fire emission inventory cannot be corrected between analysis cycles, and the model state tends to return toward its underestimated background between successive assimilation cycles. The remaining negative bias is largest during the highest observed $PM_{2.5}$ events, including the Punjab peak on 12 November and the Delhi and Meerut peaks on 17–18 November. During these periods, both DA-EXP1 and DA-EXP2 simulated $PM_{2.5}$ concentrations below the observed values, and neither experiment exactly matched the observed hourly peak concentrations. Despite these remaining limitations, both assimilation experiments, including DA-EXP1 with a realistic 10% low-cost-sensor observation error, improved the identification of observed high-AQI categories, demonstrating their value for operational early warning even when the highest hourly $PM_{2.5}$ peaks remain underestimated.

Several important limitations and directions for future work emerge from this study. First, the observation-error specification for low-cost sensors in the variational framework warrants further investigation: the optimal prescription lies between the sensor measurement uncertainty adopted in DA-EXP1 and the tight regulatory error adopted in DA-EXP2, and a physically motivated formulation that accounts for both measurement uncertainty and representativeness error at the model grid scale would improve the analysis. Expanding or relocating reference-grade monitoring stations to selected CUPI-G locations, particularly in biomass-burning source regions, could enable more accurate low-cost-sensor calibration and improve air-quality forecasts through assimilation, as indicated by the improved performance of DA-EXP2. Second, the residual underestimation points to the need for direct emission constraints — either through the assimilation of fire radiative power observations to correct biomass-burning emission source strengths in real time, or through ensemble-based approaches capable of dynamically estimating emission uncertainties within the assimilation cycle. Third, extending the assimilation to twice-daily cycles capturing both the early-morning and evening boundary layer states — as implemented here — should be retained and further optimised in future operational implementations, given the importance of the post-overpass evening emission pulse for the nocturnal $PM_{2.5}$ build-up. Finally, the approach demonstrated here can be incorporated into the operational AIRWISE system. The results provide a scientific basis for integrating dense low-cost sensor networks such as CUPI-G into the operational air-quality analysis chain over the IGP, where timely identification of extreme post-monsoon pollution episodes remains a major scientific, public-health, and regulatory challenge. Government regulations or policy guidelines should also be established to enable timely access to quality-assured air-quality measurements collected across India for scientific research and evidence-based policymaking. Such data access may be governed by appropriate terms and conditions to address data ownership, institutional requirements, quality control, and responsible use.

Methods

WRF-Chem model configuration and study domain

Atmospheric composition over northwestern India was simulated with the Weather Research and Forecasting model coupled with Chemistry (WRF-Chem, version 3.9.1), configured to reproduce the operational set-up of the Air Quality Warning and Integrated Decision Support System for Emissions (AIRWISE) developed at the Indian Institute of Tropical Meteorology[21]. The analysis was carried out on a single domain at 3 km horizontal grid spacing comprising 489 (west–east) × 335 (south–north) grid cells, centred over the crop-residue-burning belt of Punjab and Haryana and extending downwind across the Delhi National Capital Region (NCR) and the adjoining IGP. The vertical grid consisted of 60 terrain-following hybrid levels extending from the surface to [model top, e.g. 50 hPa], with the lowest layers concentrated near the ground to resolve the shallow nocturnal boundary layer that governs surface accumulation during haze episodes. The 3 km grid was chosen to resolve the sharp spatial gradients of CRB plumes, which are smeared at the coarser resolutions typical of operational forecasting[15].

Cloud microphysical processes were represented by the WRF Single-Moment 6-class scheme (WSM6[38]). Shortwave and longwave radiative transfer was treated with the Rapid Radiative Transfer Model for general circulation models (RRTMG[39]), which allows aerosols to influence the radiation field through feedback. Subgrid convective and shallow-cloud processes were handled by the scale-aware Grell–Freitas ensemble cumulus scheme[40], appropriate for the grey-zone resolution of the 3 km grid. Land-surface processes were simulated with the unified Noah land-surface model[41], and surface-layer exchange with the Monin–Obukhov (Janjić Eta) scheme[42]. Vertical subgrid-scale turbulent transport in the planetary boundary layer and free troposphere was parameterized using the Mellor–Yamada–Nakanishi–Niino level-2.5 (MYNN2.5) scheme[43].

Gas-phase chemistry was represented by the Model for Ozone and Related chemical Tracers (MOZART-4[49]) coupled to the Goddard Chemistry Aerosol Radiation and Transport (GOCART) aerosol scheme[45,46] the MOZCART configuration. GOCART simulates the major aerosol components — sulphate, black carbon, organic carbon, dust and sea salt — but in its standard form does not simulate nitrate or secondary organic aerosol (SOA), a recognized source of low bias in modelled wintertime $PM_{2.5}$ over the region[19]. Although WRF-Chem provides more complex aerosol modules that resolve nitrate and SOA, these are computationally prohibitive for operational application; the GOCART omission is therefore retained in the present configuration and is considered when interpreting the residual model–observation differences. The full set of physical and chemical parameterizations follows the operational AIRWISE configuration documented by Jena et al. (2021)[47].

Meteorological initial and lateral boundary conditions were supplied by the IITM (Indian Institute of Tropical Meteorology) Global Forecasting System (IITM-GFS, T1534) spectral model, which assimilates observations through an ensemble Kalman filter and provides fields at approximately 12.5 km resolution every three hours[48,47]. Chemical initial and lateral boundary conditions were obtained from the Whole Atmosphere Community Climate Model (WACCM)[49], which supplies time-varying global distributions of trace gases and aerosols at the domain edges. This configuration was selected intentionally because it is used in the established operational AIRWISE forecasting system at IITM. The AIRWISE system has been evaluated against other regional and global forecasting models and has demonstrated useful performance for $PM_{2.5}$ forecasting over northern India[18].

Emission inputs

Anthropogenic emissions were constructed by merging two inventories. Over the Delhi region the high-resolution (400 m) emission inventory developed under the System of Air Quality and Weather Forecasting And Research (SAFAR) project was used (http://safar.tropmet.res.in/source.pdf), while the remainder of the domain was supplied by the global EDGAR-HTAP v2.2 emissions inventory[50]. The 2010 EDGAR-HTAP emissions were first scaled to the simulation year using the sector-specific growth factors of Venkataraman et al. (2018)[51]. The native 400 m SAFAR emissions[52] were then re-gridded to the 3 km

model grid through a mass-conserving remapping that preserves the total emitted mass before and after regridding and merged with the scaled EDGAR-HTAP fields so that the fine-scale urban emission structure of Delhi is retained within the broader regional background. Biogenic emissions were computed online with the Model of Emissions of Gases and Aerosols from Nature (MEGAN[53]), and wind-blown dust was generated online using the AFWA (Air Force Weather Agency) dust-emission scheme[54]. Open biomass-burning emissions, which over this region and season are dominated by CRB, were taken from the Fire INventory from NCAR (FINN[55,56]), obtained from the NCAR Atmospheric Chemistry Observations and Modeling fire-emission archive (https://www.acom.ucar.edu/Data/fire/). FINN provides fire emissions at high spatial resolution derived from satellite-detected active fires and land-cover-specific emission factors; its known limitations during cloud- and haze-obscured days, and outside the satellite overpass window, are central to the motivation of this study.

CUPI-G observational network

Surface $PM_{2.5}$ observations were drawn from the dense low-cost sensor network operated under the Aakash project of the Research Institute for Humanity and Nature (RIHN). The network is built around the CUPI-G, which pairs a palm-sized optical $PM_{2.5}$ sensor jointly developed by Nagoya University and Panasonic with electrochemical sensors for nitric oxide, nitrogen dioxide, potential ozone (O_3 + NO_2) and carbon monoxide[16]. The optical sensor derives $PM_{2.5}$ mass concentration from the distribution of light-scattering intensities of individual particles, resolving particles down to ~ 0.3 μm and reporting reliably up to ~ 600 μg m^{-3}[29]. Each unit records at high temporal resolution and transmits data in near real time to an online server, enabling continuous monitoring throughout the burning season. Specifically, The CUPI-G sensors were deployed mainly in rural agricultural areas within the crop-residue-burning source region, especially across Punjab and Haryana, and along the downwind transport corridor toward Delhi-NCR and western Uttar Pradesh. Which is the advantage of having CUPI-G network over the reference-grade monitoring observations in Punjab and Haryana, which is mainly located in urban centres only[15].

For the present study the 2024 deployment was used, comprising sensors distributed across Punjab, Haryana, the Delhi-NCR and western Uttar Pradesh (Fig. 7). The network was deliberately sited in the rural CRB source region and along the downwind transport pathway, rather than in cities, thereby filling the spatial gap left by the urban-centric Central Pollution Control Board (CPCB) reference network and the cloud- and haze-limited satellite retrievals[16,15]. Because the sensors measure mass concentration directly at the surface, they remain available during the dense fog and haze that obscure satellite observations during peak burning, and they continue reporting through the night, when emissions accumulate under a shallow boundary layer. All quality-controlled $PM_{2.5}$ observations from the network are openly available through the Aakash data portal (https://aakash-rihn.org/en/data-set/).

The CUPI-G $PM_{2.5}$ sensors were calibrated in the laboratory before deployment against a beta attenuation mass (BAM), with a single scaling factor of ~ 1.4 applied to convert the optically derived signal to ambient mass concentration[16]. Their stability was monitored during the campaign by

intercomparison among neighbouring units and against reference instruments such as the BAM at the US Embassy, New Delhi. Laboratory tests show that the CUPI-G sensors agree closely with one another, with the sensitivity differing by less than about 10% from one unit to the next[29]. On this basis, an overall measurement uncertainty of roughly 10% of the reported concentration has been adopted for the network in earlier Aakash project studies[11]. This approximately 10% uncertainty was used to specify the observation error in the data-assimilation experiments.

Figure 7. Spatial distribution of the 33 Aakash CUPI-G low-cost sensor sites (red circles) across Punjab, Haryana and the Delhi-NCR during the November 2024 campaign.

Data assimilation framework

Surface $PM_{2.5}$ from the CUPI-G network was assimilated into WRF-Chem using the three-dimensional variational (3D-VAR) capability of the Gridpoint Statistical Interpolation (GSI) system, following the chemical data-assimilation framework of the AIRWISE system[21,57]. The 3DVAR analysis blends the model background with the observations by iteratively minimizing a cost function of the form

$$J(x) = \frac{1}{2}(x - x_b)^T B^{-1}(x - x_b) + \frac{1}{2}[y - H(x)]^T R^{-1}[y - H(x)] \quad (1)$$

where x is the analysis state vector of aerosol mass concentrations, x_b is the model background (first guess), B is the background-error covariance matrix, y is the vector of CUPI-G surface $PM_{2.5}$ observations, H is the forward observation operator that maps the GOCART aerosol species onto surface $PM_{2.5}$ space, and R is the observation-error covariance matrix that determines the relative weighting of the CUPI-G observations and the model background in the analysis. Smaller observation errors increase the influence of the observations on the analysis increment, whereas larger errors place greater weight on the model background. In contrast to conventional implementations that assimilate satellite aerosol optical depth at a single mid-day overpass (or surface $PM_{2.5}$ from the urban CPCB stations), here the assimilated constraint is the source-region, all-weather CUPI-G surface network. During each analysis only the GOCART species that contribute to $PM_{2.5}$ are adjusted[47].

The background-error covariance (BEC) matrix used in the GSI assimilation was estimated using the National Meteorological Center (NMC) method through the Generalized Background Error (GEN_BE) utility[58]. The same methodology was followed for both the 00 UTC and 15 UTC assimilation cycles. In this approach, pairs of WRF-Chem forecasts valid at the same analysis time were generated using different meteorological inputs and perturbed anthropogenic and biomass-burning emissions. Following previous applications over northern India, 100% uncertainty was assumed for both anthropogenic and biomass-burning emissions to represent the large emission uncertainty during the crop-residue-burning season. The differences between paired forecasts were then used by GEN_BE to estimate the background-error variances and the horizontal and vertical length scales. The variance controls the magnitude of the analysis increment produced from the model–observation innovation, while the length scales determine how the increment is spread horizontally and vertically to neighbouring grid cells. Thus,

the BEC used in the 00 UTC and 15 UTC analyses accounts for uncertainties in both meteorology and emissions at the respective assimilation times. The observation error for CUPI-G $PM_{2.5}$ was prescribed according to the experimental design, using either a concentration-dependent error based on the reported sensor accuracy or a fixed error assumption, to examine the sensitivity of the analysis to the specified observational uncertainty.

Simulation setup and experiments

The model simulations were carried out for a 12-day analysis period from 10 to 21 November 2024, representing the peak post-monsoon biomass-burning and pollution episode over northwest India. Before the start of this analysis period, each simulation was initialized with a 7-day spin-up beginning on 3 November 2024. This spin-up period allowed the meteorological and chemical fields to adjust before the assimilation experiments began on 10 November 2024. During the analysis period, meteorology was reinitialized daily from the IITM-GFS forecast, while the chemical fields were carried forward from the previous cycle to maintain continuity in aerosol and trace-gas concentrations.

Each model integration was preceded by a 7-day spin-up beginning on 3 November 2024, allowing the meteorological and chemical fields to reach dynamical and chemical equilibrium before the 10 November start of the analysis window. Through the analysis period the model was cycled with daily reinitialization of the meteorology from the IITM-GFS forecast, while the chemical fields were carried forward from the previous cycle to preserve aerosol memory.

Three experiments were performed: a control (CNTL) simulation without assimilation (the model background), and two assimilation experiments that are identical in every respect except for the assumed observation error, which controls how strongly the analysis is drawn toward the low-cost observations. In the first assimilation experiment (DA-EXP1) the observation error was set to 10% of each observed concentration, consistent with the measurement uncertainty of the low-cost sensors. In the second experiment (DA-EXP2) the observation error was instead fixed at 1.5 μg m^{-3} — the value specified for the CPCB surface $PM_{2.5}$ observations assimilated in the AIRWISE system[21]. DA-EXP2 thus applies to the low-cost network the same observation error that AIRWISE assigns to regulatory-grade CPCB monitors. Comparing DA-EXP1 and DA-EXP2 therefore isolates how the recovered episode depends on the assumed accuracy of the assimilated data — specifically, whether weighting the CUPI-G observations by their own ~ 10% uncertainty, rather than by the much tighter CPCB error used operationally, changes the analysis.

Model evaluation and AQI assessment

Model performance was evaluated against the CUPI-G surface $PM_{2.5}$ observations using four standard metrics: the root-mean-square error (RMSE), the mean fractional bias (MFB), the normalized mean bias (NMB) and the index of agreement (IOA). RMSE quantifies the absolute magnitude of the error; MFB and NMB characterize the systematic over- or under-prediction in fractional and normalized terms, respectively, and are symmetric and bounded measures suited to concentrations spanning a wide dynamic range; and IOA measures the overall agreement between the modelled and observed time

series, with values approaching unity indicating closer correspondence[59,60,61]. The formulas used to compute these metrics are provided in the Supplementary Document. These metrics were computed for the control and assimilation experiments to quantify the improvement in surface $PM_{2.5}$ attributable to assimilating the low-cost network.

Because the operational value of a forecast lies in the air-quality category derived from the absolute $PM_{2.5}$ concentration, the simulated and observed $PM_{2.5}$ were additionally converted to the Air Quality Index (AQI) using the Central Pollution Control Board (CPCB) breakpoint concentrations for 24-hour $PM_{2.5}$. These breakpoints define six classes, each spanning an AQI index range and a corresponding 24-hour $PM_{2.5}$ concentration range (μg m^{-3}): good (AQI 0–50; $PM_{2.5}$ 0–30), satisfactory (AQI 51–100; $PM_{2.5}$ 30–60), moderate (AQI 101–200; $PM_{2.5}$ 60–90), poor (AQI 201–300; $PM_{2.5}$ 90–120), very poor (AQI 301–400; $PM_{2.5}$ 120–250) and severe (AQI 401+; $PM_{2.5}$ 250+). The skill of each experiment was then assessed categorically rather than continuously: for every observed AQI class, we computed the percentage of time steps at which the experiment placed $PM_{2.5}$ in that same class (Eq. 2), conditioned on the observation falling in that class. This conditional match rate is the relevant measure for operational forecasting, because it is the predicted AQI category which trigger Graded Response Action Plan (GRAP) interventions; A model that misses the observed category provides no actionable information. The evaluation thus tests whether assimilating the low-cost network enables the model to place the episode in the correct AQI class on the most polluted days (very poor and severe), when the control simulation underestimates the magnitude of the haze and consequently fails to register the correct category.

$$CM_e\left(c\right) = \frac{N_{match}\left(c\right)}{N_{obs}\left(c\right)} \times 100$$

2

where CMe(c) is the AQI category match percentage (%) for experiment “e” (e ∈ {CNTL, DA-EXP1, DA-EXP2}) and AQI category “c” (c ∈ {good, satisfactory, moderate, poor, very poor, severe}); Nobs(c) is the total number of time steps at which the observation belonged to category “c”; and Nmatch, “e(c)” is the number of timestamps at which the experiment “e” belonged to category “c”. By construction CMe(c) ranges from 0% (the experiment never reproduces the observed category) to 100% (the experiment reproduces it at every timestamp it occurs).

Data Availability

The CUPI-G hourly averaged $PM_{2.5}$ observations used in this study are publicly available through the Aakash Project data portal of the Research Institute for Humanity and Nature (RIHN) at https://aakash-rihn.org/en/data-set/. Aerosol Optical Depth (AOD) data from the Ocean Colour Monitor (OCM) onboard Oceansat-3/EOS-06 were obtained from the Indian Space Research Organisation (ISRO) and are available through the MOSDAC (Meteorological and Oceanographic Satellite Data Archival Centre) portal

(https://www.mosdac.gov.in/). Model output data and processed datasets generated during this study are available from the corresponding author upon reasonable request.

Code availability

The WRF model and the software used for data analysis are open source. Data processing and analysis in this study were performed using Python and other standard open-source tools. The analysis codes are available from the corresponding author upon reasonable request.

Declarations

Contributions

P.P.Y. and S.D.G. conceived and designed the study. P.P.Y. performed the WRF-Chem simulations, implemented the data-assimilation experiments, analysed the data, prepared the figures, and wrote the original draft. R.J., G.G., and R.K. contributed to the study design, data-assimilation methodology, model development, and interpretation of the results. P.K.P., Y.M., T.N., and S.H. contributed to the CUPI-G observation network, observational data, data curation, and interpretation. A.R. and V.K. contributed to model simulations, data processing, and analysis. S.D.G. supervised the study and contributed to the interpretation, review, and editing of the manuscript. All authors reviewed, edited, and approved the final version of the manuscript.

Competing interests

The authors declare no financial or non-financial competing interests.

Author Contribution

P.P.Y. and S.D.G. conceived and designed the study. P.P.Y. performed the WRF-Chem simulations, implemented the data-assimilation experiments, analysed the data, prepared the figures, and wrote the original draft. R.J., G.G., and R.K. contributed to the study design, data-assimilation methodology, model development, and interpretation of the results. P.K.P., Y.M., T.N., and S.H. contributed to the CUPI-G observation network, observational data, data curation, and interpretation. A.R.,V.K. and C.J contributed to model simulations, data processing, and analysis. S.D.G. supervised the study and contributed to the interpretation, review, and editing of the manuscript. All authors reviewed, edited, and approved the final version of the manuscript.

Acknowledgement

Aakash Project is financially supported by the Research Institute for Humanity and Nature (RIHN: a constituent member of NIHU) Project No. 14200133. Aakash Project's CUPI-G measurements are supported by Sanjeev Bhardwaj (Department of Environment Studies, Panjab University, Chandigarh, India), Manpreet S. Bhatti (Department of Botanical and Environmental Sciences, Guru Nanak Dev University, Amritsar, Punjab, India), Surendra K. Dhaka (Radio and Atmospheric Physics Lab, Rajdhani College, University of Delhi, New Delhi, India), A. P. Dimri (School of Environmental Sciences, Jawaharlal Nehru University, New Delhi, India), Ravi K. Kunchala (Centre for Atmospheric Sciences, Indian Institute of Technology Delhi, New Delhi, India), Shristy Malik (Department of Applied Physics, Delhi Technological University, Delhi, India), Tuhin K. Mandal (Environmental Sciences & Biomedical Metrology Division, CSIR-National Physical Laboratory, New Delhi, India), Prakhar Misra (Dept. of Civil Engineering, Indian Institute of Technology Roorkee, Uttarakhand, India), Sahil Mor (Department of Environmental Science Engineering, Guru Jambheshwar University of Science and Technology, Hisar, India), Suman Mor (Department of Environment Studies, Panjab University, Chandigarh, India), Manish K. Naja (Aryabhatta Research Institute of Observational Sciences, Manora Peak, Nainital, Uttarakhand, India), Khaiwal Ravindra (Department of Community Medicine and School of Public Health, Postgraduate Institute of Medical Education and Research, Chandigarh, India), Aka Sharma (School of Environmental Sciences, Jawaharlal Nehru University, New Delhi, India), Tanbir Singh (SCVB Government College, Palampur, Himachal Pradesh, India), Kamal Vatta (Department of Economics and Sociology, Punjab Agricultural University, Ludhiana, Punjab, India), Natsuko Yasutomi, Hikaru Araki, Poonam Mangaraj and Akash Biswal (Research Institute for Humanity and Nature, Kyoto, Japan), and members at the Centers for International Projects Trust (CIPT), Ludhiana. The OCM aerosol optical depth data were obtained from the Indian Space Research Organisation (ISRO). The FINN fire emission inventory was obtained from the NCAR Atmospheric Chemistry Observations and Modeling (ACOM) Laboratory fire-emission archive. The contributions of Rajesh Kumar were supported by the National Science Foundation National Center for Atmospheric Research (NSF NCAR), a facility sponsored by the U.S. National Science Foundation under Agreement No. 1852977, and the NASA Health and Air Quality program (Grant No. 80NSSC22K1045). The authors gratefully acknowledge the use of computational resources at Pratyush for conducting the WRF-Chem simulations presented in this study.

References

1. Snyder, E. G., Watkins, T. H., Solomon, P. A., Thoma, E. D., Williams, R. W., Hagler, G. S. W., et al.: The changing paradigm of air pollution monitoring, Environ. Sci. Technol., 47, 11369–11377, https://doi.org/10.1021/es4022602, 2013.
2. Bhuyan, A., Bordoloi, T., Debnath, R., Ikbal, A. M. A., Debnath, B., and Singh, W. S.: Assessing AQI of air pollution crisis 2024 in Delhi: its health risks and nationwide impact, Discover Atmosphere, 3, 13, https://doi.org/10.1007/s44292-025-00041-x, 2025.
3. Ghude, S. D., Chate, D. M., Jena, C., Beig, G., Kumar, R., Barth, M. C., et al.: Premature mortality in India due to $PM_{2.5}$ and ozone exposure, Geophys. Res. Lett., 43, 4650–4658, https://doi.org/10.1002/2016GL068949, 2016.

4. Pandey, A., Brauer, M., Cropper, M. L., Balakrishnan, K., Mathur, P., Dey, S., et al.: Health and economic impact of air pollution in the states of India: the Global Burden of Disease Study 2019, Lancet Planet. Health, 5, e25–e38, https://doi.org/10.1016/S2542-5196(20)30298-9, 2021.
5. Jat, R., Gurjar, B. R., and Lowe, D.: Regional pollution loading in winter months over India using high resolution WRF-Chem simulation, Atmos. Res., 249, 105326, https://doi.org/10.1016/j.atmosres.2020.105326, 2021.
6. Govardhan, G., Ghude, S. D., Kumar, R., Sharma, S., Gunwani, P., Jena, C., Yadav, P., Ingle, S., Debnath, S., Pawar, P., Acharja, P., Jat, R., Kalita, G., Ambulkar, R., Kulkarni, S., Kaginalkar, A., Soni, V. K., Nanjundiah, R. S., and Rajeevan, M.: Decision Support System version 1.0 (DSS v1.0) for air quality management in Delhi, India, Geosci. Model Dev., 17, 2617–2640, https://doi.org/10.5194/gmd-17-2617-2024, 2024.
7. Singh, N., Pradhan, R., Shukla, B.P., Pandya, M.R., 2025. Evidence of shift in stubble burning timing over northwest India from geostationary satellite observations. Curr. Sci. 129 (10), 921–923. https://doi.org/10.18520/cs/v129/i10/921-923
8. Liu, T., et al.: Crop residue burning practices across north India inferred from household survey data: Bridging gaps in satellite observations, Atmos. Environ.: X, 8, 100091, https://doi.org/10.1016/j.aeaoa.2020.100091, 2020.
9. Govardhan, G., Ambulkar, R., Kulkarni, S., Vishnoi, A., Yadav, P., Choudhury, B. A., Khare, M., and Ghude, S. D.: Stubble-burning activities in north-western India in 2021: Contribution to air pollution in Delhi, Heliyon, 9, e16939, https://doi.org/10.1016/j.heliyon.2023.e16939, 2023.
10. Singh, T., et al.: A high-resolution emission inventory of air pollutants from primary crop residue burning over Northern India based on VIIRS thermal anomalies, Environ. Pollut., 266, 115132, https://doi.org/10.1016/j.envpol.2020.115132, 2020.
11. Biswal, A., Takigawa, M., Mangaraj, P., Bisht, J. S. H., Patra, P. K., Matsumi, Y., Nakayama, T., Araki, H., Yasutomi, N., Singh, V., and the Aakash CUPI-G team: Emission time and amount of crop residue burning play critical role on $PM_{2.5}$ variability during October–November in northwestern India during 2022–2024, Environ. Sci.: Atmos., 5, 1211–1229, https://doi.org/10.1039/d5ea00052a, 2025.
12. Ghude, S.D., Kalita, G., Jat, R. et al. The role of atmospheric feedback and groundwater conservation policies in degrading air quality in Delhi. npj Clean Air 1, 12 (2025). https://doi.org/10.1038/s44407-025-00012-x
13. Sawlani, R., et al.: The severe Delhi smog of 2016: a case of delayed crop residue burning, coincident firecracker emissions, and atypical meteorology, Atmos. Pollut. Res., 10, 868–879, https://doi.org/10.1016/j.apr.2018.12.015, 2019.
14. Sengupta, A., Govardhan, G., Debnath, S., Yadav, P., Kulkarni, S. H., Parde, A. N., et al.: Probing into the wintertime meteorology and particulate matter ($PM_{2.5}$ and PM_{10}) forecast over Delhi, Atmos. Pollut. Res., 13, 101426, https://doi.org/10.1016/j.apr.2022.101426, 2022.
15. Mangaraj, P., Matsumi, Y., Nakayama, T., Biswal, A., Yamaji, K., Araki, H., et al.: Weak coupling of observed surface $PM_{2.5}$ in Delhi-NCR with rice crop residue burning in Punjab and Haryana, npj Clim.

Atmos. Sci., 8, 18, https://doi.org/10.1038/s41612-025-00901-8, 2025.

16. Singh, T., Matsumi, Y., Nakayama, T., Hayashida, S., Patra, P. K., Yasutomi, N., et al.: Very high particulate pollution over northwest India captured by a high-density in situ sensor network, Sci. Rep., 13, 13201, https://doi.org/10.1038/s41598-023-39471-1, 2023.
17. Yadav, P., Parde, A.N., Dhangar, N.G. et al. Understanding the genesis of a dense fog event over Delhi using observations and high-resolution model experiments. Model. Earth Syst. Environ. 8, 5011–5022 (2022). https://doi.org/10.1007/s40808-022-01463-x
18. Yadav, P. P., Jat, R., Ghude, S. D., Govardhan, G., Kumar, R., Debnath, S., et al.: Evaluating the performance of regional and global forecasting models for accurate $PM_{2.5}$ prediction and air quality index assessment in Delhi, India, J. Geophys. Res. Atmos., 130, e2025JD043719, 2025a.
19. Jat, R., Vispute, A. S., Ghude, S. D., Kumar, R., Sinha, V., Sinha, B., et al.: Implementation and evaluation of an observation-constrained secondary organic aerosol parameterization in MOZART–GOCART chemistry in WRF-Chem, EGUsphere [preprint], https://doi.org/10.5194/egusphere-2026-1302, 2026.
20. Kumar, R., Ghude, S. D., Biswas, M., Jena, C., Alessandrini, S., Debnath, S., et al.: Enhancing accuracy of air quality and temperature forecasts during paddy crop residue burning season in Delhi via chemical data assimilation, J. Geophys. Res. Atmos., 125, e2020JD033019, https://doi.org/10.1029/2020JD033019, 2020.
21. Ghude, S. D., Govardhan, G., Kumar, R., Yadav, P. P., Jat, R., Debnath, S., et al.: Air Quality Warning and Integrated Decision Support System for Emissions (AIRWISE): Enhancing air quality management in megacities, Bull. Am. Meteorol. Soc., 105, E2525–E2550, https://doi.org/10.1175/BAMS-D-23-0181.1, 2024.
22. Kumar, R., Meech, S., Yadav, P. P., Cheng, W. Y. Y., Ghude, S. D., Alessandrini, S., Jat, R., and Govardhan, G.: Will assimilating VIIRS AOD data improve New Delhi's air pollution forecasts as much as assimilating MODIS AOD?, Atmos. Environ., 361, 121526, https://doi.org/10.1016/j.atmosenv.2025.121526, 2025.
23. Yadav, P. P., Ghude, S. D., Govardhan, G., et al.: Implementation of MOPITT carbon monoxide (CO) data assimilation in WRF-Chem for improving CO analysis over India, Sci. Rep., 2026.
24. Kumar, P., Morawska, L., Martani, C., Biskos, G., Neophytou, M., Di Sabatino, S., et al.: The rise of low-cost sensing for managing air pollution in cities, Environ. Int., 75, 199–205, https://doi.org/10.1016/j.envint.2014.11.019, 2015.
25. Morawska, L., Thai, P. K., Liu, X., Asumadu-Sakyi, A., Ayoko, G., Bartonova, A., et al.: Applications of low-cost sensing technologies for air quality monitoring and exposure assessment: How far have they gone?, Environ. Int., 116, 286–299, https://doi.org/10.1016/j.envint.2018.04.018, 2018.
26. Schmitz, S., von Schneidemesser, E. Harness low-cost sensors for the targeted assessment of policy. npj Clim Atmos Sci 8, 360 (2025). https://doi.org/10.1038/s41612-025-01200-y
27. Bagkis, E., Hassani, A., Schneider, P. et al. Evolving trends in application of low-cost air quality sensor networks: challenges and future directions. npj Clim Atmos Sci 8, 335 (2025).

https://doi.org/10.1038/s41612-025-01216-4

28. Brauer, M., Freedman, G., Frostad, J., van Donkelaar, A., Martin, R. V., Dentener, F., et al.: Ambient air pollution exposure estimation for the Global Burden of Disease 2019, Environ. Sci. Technol., 53, 123–134, 2019.
29. Nakayama, T., Matsumi, Y., Kawahito, K., and Watabe, Y.: Development and evaluation of a palm-sized optical $PM_{2.5}$ sensor, Aerosol Sci. Technol., 52, 2–12, https://doi.org/10.1080/02786826.2017.1375078, 2018.
30. Aung, H. K. Z. Z., Boontanon, S. K., Li, J., Sakamoto, Y., Boontanon, N., and Kajii, Y.: Air quality analysis in the selected urban and suburban areas in central Thailand by Compact and Useful $PM_{2.5}$ Instrument with Gas sensors (CUPI-G), Thai Environ. Eng. J., 37(2), 77–88, 2023.
31. Kajino, M., Deushi, M., Sekiyama, T.T., Oshima, N., Yumimoto, K., Tanaka, T.Y., Ching, J., Hashimoto, A., Yamamoto, T., Ikegami, M., Kamada, A., Miyashita, M., Inomata, Y., Shima, S.-i., Takami, A., Shimizu, A., Hatakeyama, S., Sadanaga, Y., Irie, H., Adachi, K., Zaizen, Y., Igarashi, Y., Ueda, H., Maki, T., Mikami, M., 2019. NHM-Chem, the Japan Meteorological Agency's regional meteorology–chemistry model: Model evaluations toward the consistent predictions of the chemical, physical, and optical properties of aerosols. J. Meteorol. Soc. Jpn. Ser. II 97 (2), 337–374. https://doi.org/10.2151/jmsj.2019-020
32. Guttikunda, S. K. and Calori, G.: A GIS based emissions inventory at 1 km × 1 km spatial resolution for air pollution analysis in Delhi, India, Atmos. Environ., 67, 101–111, https://doi.org/10.1016/j.atmosenv.2012.10.040, 2013.
33. Kaskaoutis, D. G., Kumar, S., Sharma, D., Singh, R. P., Kharol, S. K., Sharma, M., Singh, A. K., Singh, S., Singh, A., and Singh, D.: Effects of crop residue burning on aerosol properties, plume characteristics, and long-range transport over northern India, J. Geophys. Res. Atmos., 119, 5424–5444, https://doi.org/10.1002/2013JD021357, 2014.
34. Srivastava, A. K., Singh, S., Tiwari, S., and Bisht, D. S.: Contribution of anthropogenic aerosols in direct radiative forcing and atmospheric heating rate over Delhi in the Indo-Gangetic Plain, Environ. Sci. Pollut. Res., 19, 1144–1158, https://doi.org/10.1007/s11356-011-0633-y, 2012.
35. Cusworth, D. H., Mickley, L. J., Sulprizio, M. P., Liu, T., Marlier, M. E., DeFries, R. S., Guttikunda, S. K., and Gupta, P.: Quantifying the influence of agricultural fires in northwest India on urban air pollution in Delhi, India, Environ. Res. Lett., 13, 044018, https://doi.org/10.1088/1748-9326/aab303, 2018.
36. Ojha, N., Sharma, A., Kumar, M., Girach, I., Ansari, T. U., Sharma, S. K., Singh, N., Pozzer, A., and Gunthe, S. S.: On the widespread enhancement in fine particulate matter across the Indo-Gangetic Plain towards winter, Sci. Rep., 10, 5862, https://doi.org/10.1038/s41598-020-62710-8, 2020.
37. Mhawish, A., Banerjee, T., Broday, D. M., Misra, A., and Tripathi, S. N.: Evaluation of MODIS Collection 6 aerosol retrieval algorithms over Indo-Gangetic Plain: Implications of aerosol types and surface reflectance, Remote Sens. Environ., 201, 297–313, https://doi.org/10.1016/j.rse.2017.09.016, 2019.
38. Hong, S.-Y. and Lim, J.-O. J.: The WRF Single-Moment 6-Class Microphysics Scheme (WSM6), J. Korean Meteorol. Soc., 42, 129–151, 2006.

39. Iacono, M. J., Delamere, J. S., Mlawer, E. J., Shephard, M. W., Clough, S. A., and Collins, W. D.: Radiative forcing by long-lived greenhouse gases: Calculations with the AER radiative transfer models, J. Geophys. Res., 113, D13103, https://doi.org/10.1029/2008JD009944, 2008.
40. Grell, G. A. and Freitas, S. R.: A scale and aerosol aware stochastic convective parameterization for weather and air quality modeling, Atmos. Chem. Phys., 14, 5233–5250, https://doi.org/10.5194/acp-14-5233-2014, 2014.
41. Tewari, M., Chen, F., Wang, W., Dudhia, J., LeMone, M. A., Mitchell, K., et al.: Implementation and verification of the unified NOAH land surface model in the WRF model, Proc. 20th Conf. on Weather Analysis and Forecasting/16th Conf. on Numerical Weather Prediction, Seattle, WA, USA, 2004.
42. Janjić, Z. I.: Nonsingular implementation of the Mellor–Yamada level 2.5 scheme in the NCEP Meso model, NCEP Office Note No. 437, 61 pp., 2001.
43. Nakanishi, M. and Niino, H.: An improved Mellor–Yamada level-3 model with condensation physics: Its design and verification, Bound.-Layer Meteorol., 119, 397–407, https://doi.org/10.1007/s10546-005-9030-8, 2006.
44. Emmons, L. K., Walters, S., Hess, P. G., Lamarque, J.-F., Pfister, G. G., and Fillmore, D., et al.: Description and evaluation of the Model for Ozone and Related Chemical Tracers, version 4 (MOZART-4), Geosci. Model Dev., 3, 43–67, 2010.
45. Chin, M., Rood, R. B., Lin, S.-J., Müller, J.-F., and Thompson, A. M.: Atmospheric sulfur cycle simulated in the global model GOCART: Model description and global properties, J. Geophys. Res., 105, 24671–24687, 2000.
46. Ginoux, P., Chin, M., Tegen, I., Prospero, J. M., Holben, B., Dubovik, O., and Lin, S.-J.: Sources and distributions of dust aerosols simulated with the GOCART model, J. Geophys. Res., 106, 20255–20273, 2001.
47. Jena, C., Ghude, S. D., Kumar, R., Debnath, S., Govardhan, G., Soni, V. K., et al.: Performance of high resolution (400 m) $PM_{2.5}$ forecast over Delhi, Sci. Rep., 11, 4104, https://doi.org/10.1038/s41598-021-83467-8, 2021.
48. Mukhopadhyay, P., et al.: Performance of a very high-resolution global forecast system model (GFS T1534) at 12.5 km over the Indian region during the 2016–2017 monsoon seasons, J. Earth Syst. Sci., 128, 155, 2019.
49. Emmons, L. K., Schwantes, R. H., Orlando, J. J., Tyndall, G., Kinnison, D., Lamarque, J.-F., et al.: The Chemistry Mechanism in the Community Earth System Model version 2 (CESM2), J. Adv. Model. Earth Syst., 12, e2019MS001882, 2020.
50. Janssens-Maenhout, G., Crippa, M., Guizzardi, D., Dentener, F., Muntean, M., and Pouliot, G., et al.: HTAP_v2.2: A mosaic of regional and global emission grid maps for 2008 and 2010, JRC Technical Report, European Commission, 2015.10.1007/s44292-025-00041-x
51. Venkataraman, C., Brauer, M., Tibrewal, K., Sadavarte, P., Ma, Q., Cohen, A., et al.: Source influence on emission pathways and ambient $PM_{2.5}$ pollution over India (2015–2050), Atmos. Chem. Phys., 18, 8017–8039, https://doi.org/10.5194/acp-18-8017-2018, 2018.

52. Beig, G., and Coauthors, 2018: SAFAR-high resolution emission inventory of Megacity Delhi for 2018. IITM, Ministry of Earth Sciences Special Scientific Rep. SAFAR-Delhi-2018-A, 71 pp., https://questionofcities.org/wp-content/uploads/2022/11/SAFAR-High-Resolution-Emission-Inventory-of-Mega-City-Delhi-2018.pdf.
53. Guenther, A. B., Jiang, X., Heald, C. L., Sakulyanontvittaya, T., Duhl, T., Emmons, L. K., and Wang, X.: The Model of Emissions of Gases and Aerosols from Nature version 2.1 (MEGAN2.1): An extended and updated framework for modeling biogenic emissions, Geosci. Model Dev., 5, 1471–1492, https://doi.org/10.5194/gmd-5-1471-2012, 2012.
54. Jones, S. L. and Creighton, G. A.: AFWA Dust Emission Scheme for the WRF-Chem Model, Air Force Weather Agency Technical Report, 2011.
55. Wiedinmyer, C., Akagi, S. K., Yokelson, R. J., Emmons, L. K., Al-Saadi, J. A., Orlando, J. J., and Soja, A. J.: The Fire Inventory from NCAR (FINN): A high-resolution global model to estimate emissions from open burning, Geosci. Model Dev., 4, 625–641, https://doi.org/10.5194/gmd-4-625-2011, 2011.
56. Wiedinmyer, C., Kimura, Y., McDonald-Buller, E. C., Emmons, L. K., Buchholz, R. R., Tang, W., et al.: The Fire Inventory from NCAR version 2.5: an updated global fire emissions model for climate and chemistry applications, Geosci. Model Dev., 16, 3873–3891, https://doi.org/10.5194/gmd-16-3873-2023, 2023.
57. Yadav, P. P., Ghude, S. D., Kumar, R., et al.: Assimilation of high-resolution Ocean Color Monitor (OCM) aerosol optical depth in WRF-Chem improves $PM_{2.5}$ forecasts over the Indian region, Sci. Rep., 15, 39669, 2025b.
58. Parrish, D. F. and Derber, J. C.: The National Meteorological Center's spectral statistical interpolation analysis system, Mon. Weather Rev., 120, 1747–1763, 1992.
59. Willmott, C. J.: On the validation of models, Phys. Geogr., 2, 184–194, 1981.
60. Boylan, J. W. and Russell, A. G.: PM and light extinction model performance metrics, goals, and criteria for three-dimensional air quality models, Atmos. Environ., 40, 4946–4959, 2006.
61. Yu, S., Eder, B., Dennis, R., Chu, S.-H., and Schwartz, S. E.: New unbiased symmetric metrics for evaluation of air quality models, Atmos. Sci. Lett., 7, 26–34, https://doi.org/10.1002/asl.125, 2006.

Figures

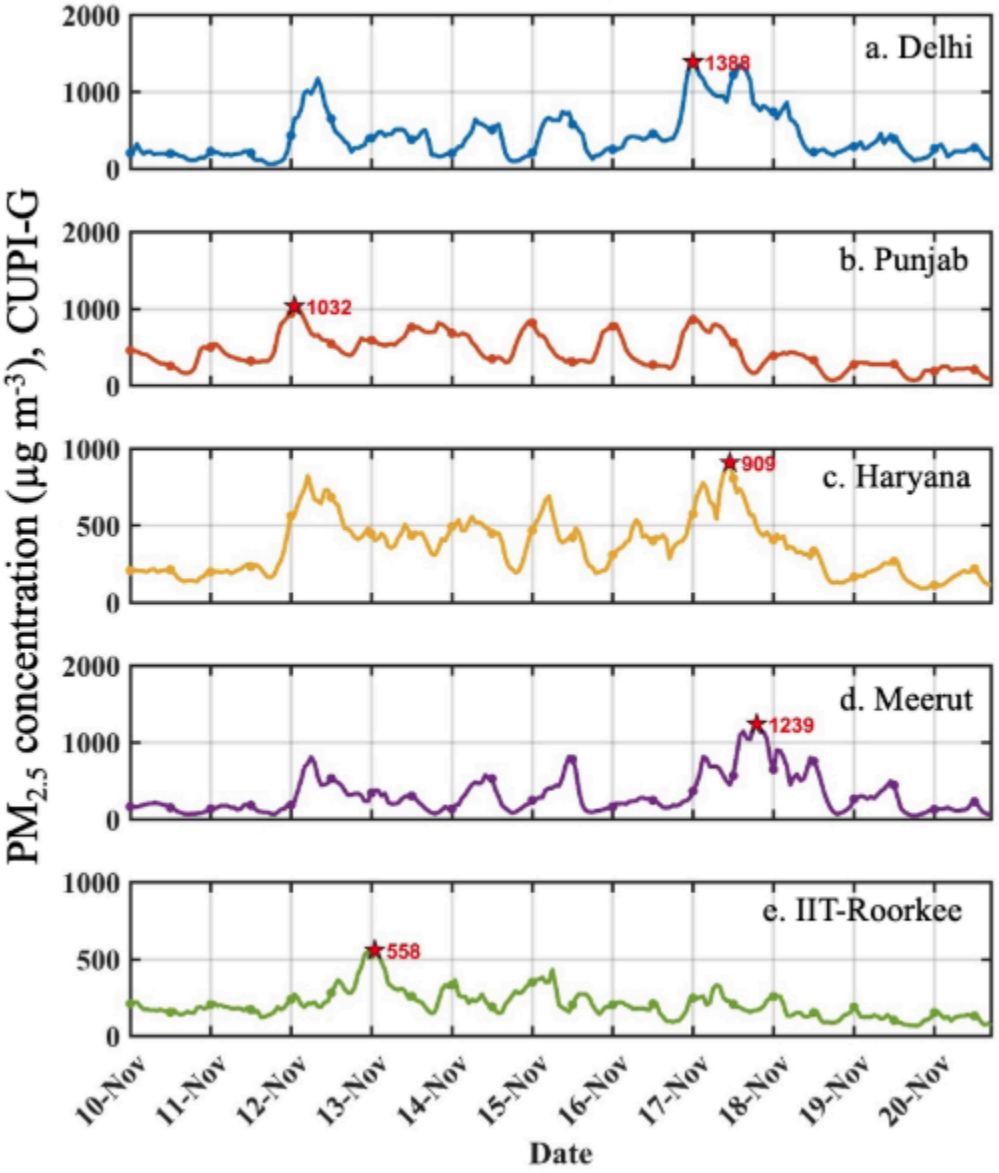


Figure 1

Hourly surface $PM_{2.5}$ (µg m^{-3}) observed by the CUPI-G network from 10 to 21 November 2024, averaged over 33 stations spread across five regions: Delhi, Punjab, Haryana, Meerut and IIT-Roorkee (top to bottom). The red star in each panel marks the maximum value attained during the period, with its magnitude annotated in red. Note that the y-axis range differs between panels (0–2000 µg m^{-3} for Delhi, Punjab and Meerut; 0–1000 µg m^{-3} for Haryana and IIT-Roorkee).

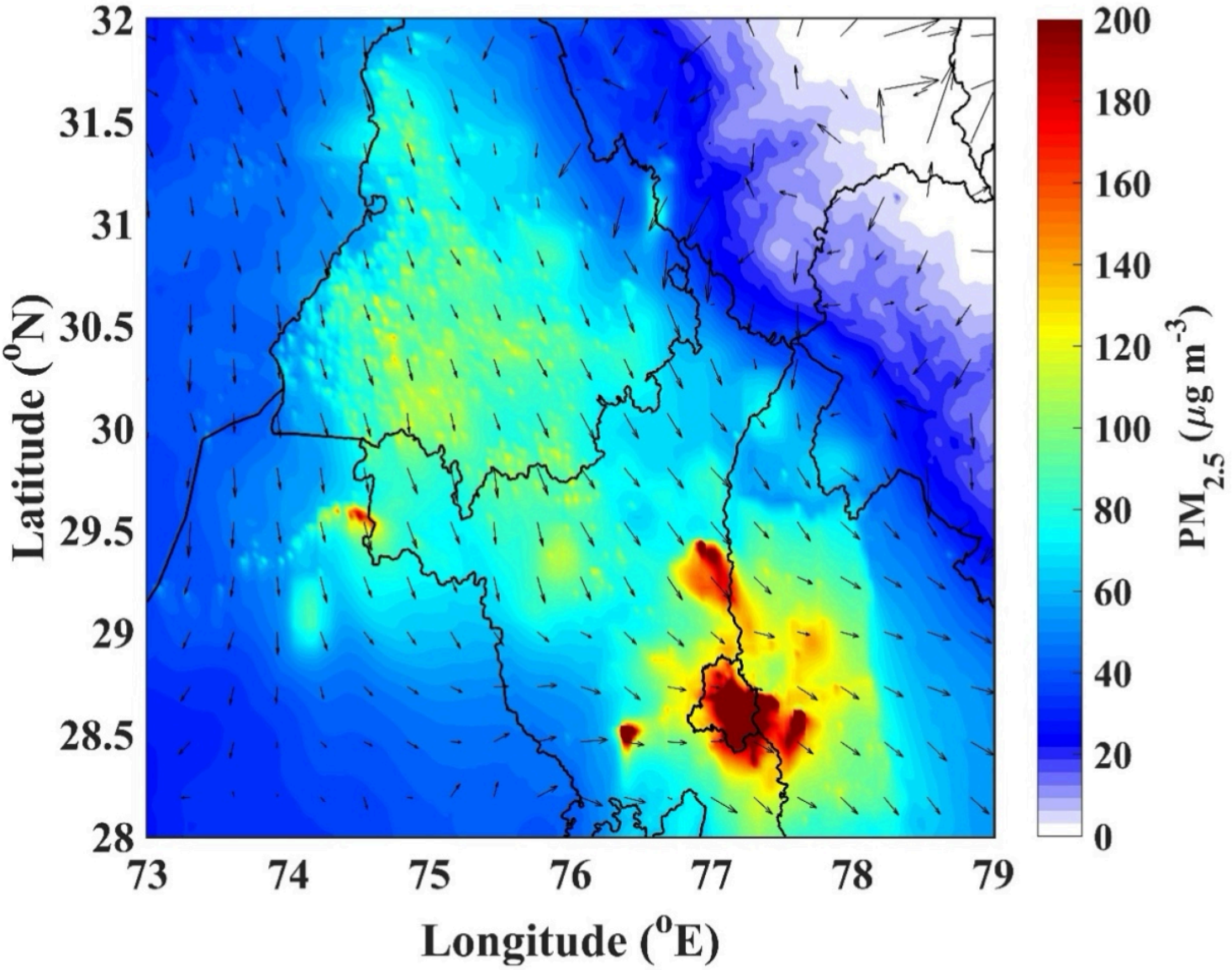


Figure 2

Mean surface $PM_{2.5}$ concentration (μg m^{-3}; shaded) overlaid with 10 m wind vectors, averaged over 10–21 November 2024, from the DA-EXP2 assimilation experiment over the analysis domain. The north-westerly low-level flow advects pollution from the Punjab and Haryana CRB source regions toward Delhi-NCR and the downwind areas to the southeast.

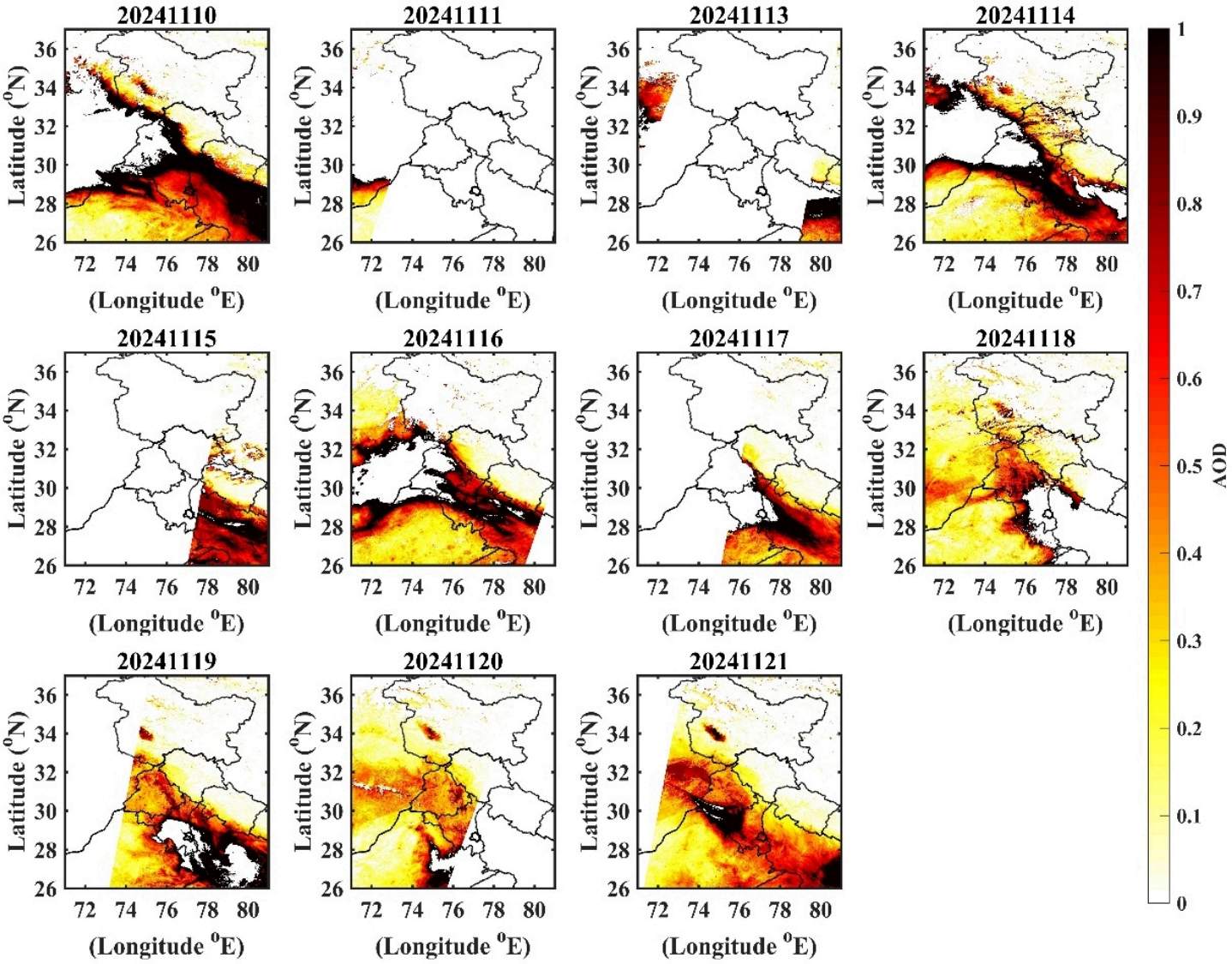


Figure 3

Daily OCM AOD over the study region, 10–21 November 2024. White areas are missing retrievals; the extensive gaps over the Indo-Gangetic Plain reflect dense fog, haze and low cloud that preclude reliable AOD retrieval during the episode.

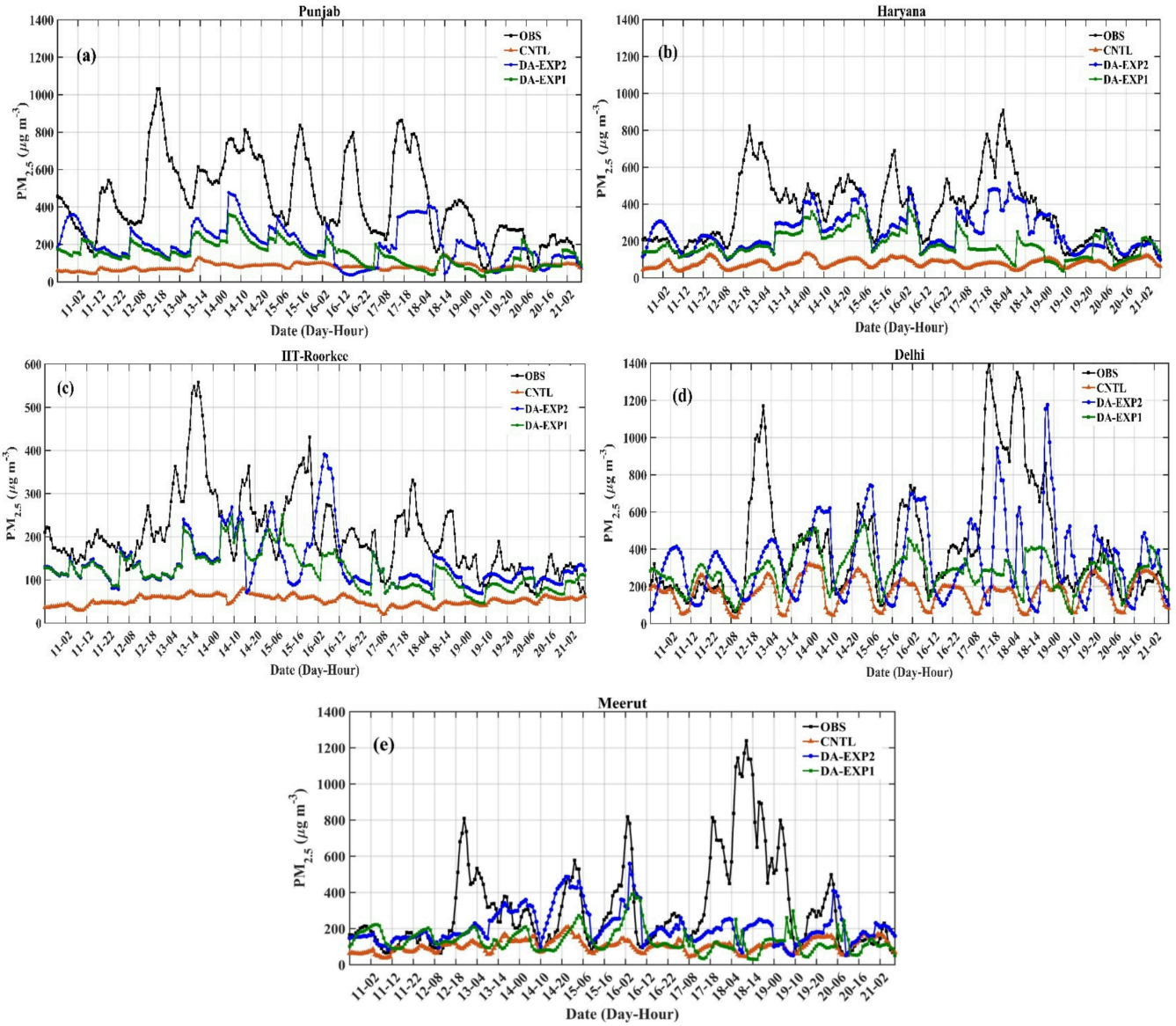


Figure 4

Time series of hourly surface $PM_{2.5}$ concentrations (μg m^{-3}) for the five regions: (a) Punjab, (b) Haryana, (c) IIT-Roorkee, (d) Delhi, and (e) Meerut, over the period 10–21 November 2024. The black line represents the observed $PM_{2.5}$ (OBS), the orange line the control simulation (CNTL), the blue line the assimilation experiment with a fixed observation error of 1.5 μg m^{-3} (DA-EXP2), and the green line the assimilation experiment with an observation error of 10% of the observed value (DA-EXP1).

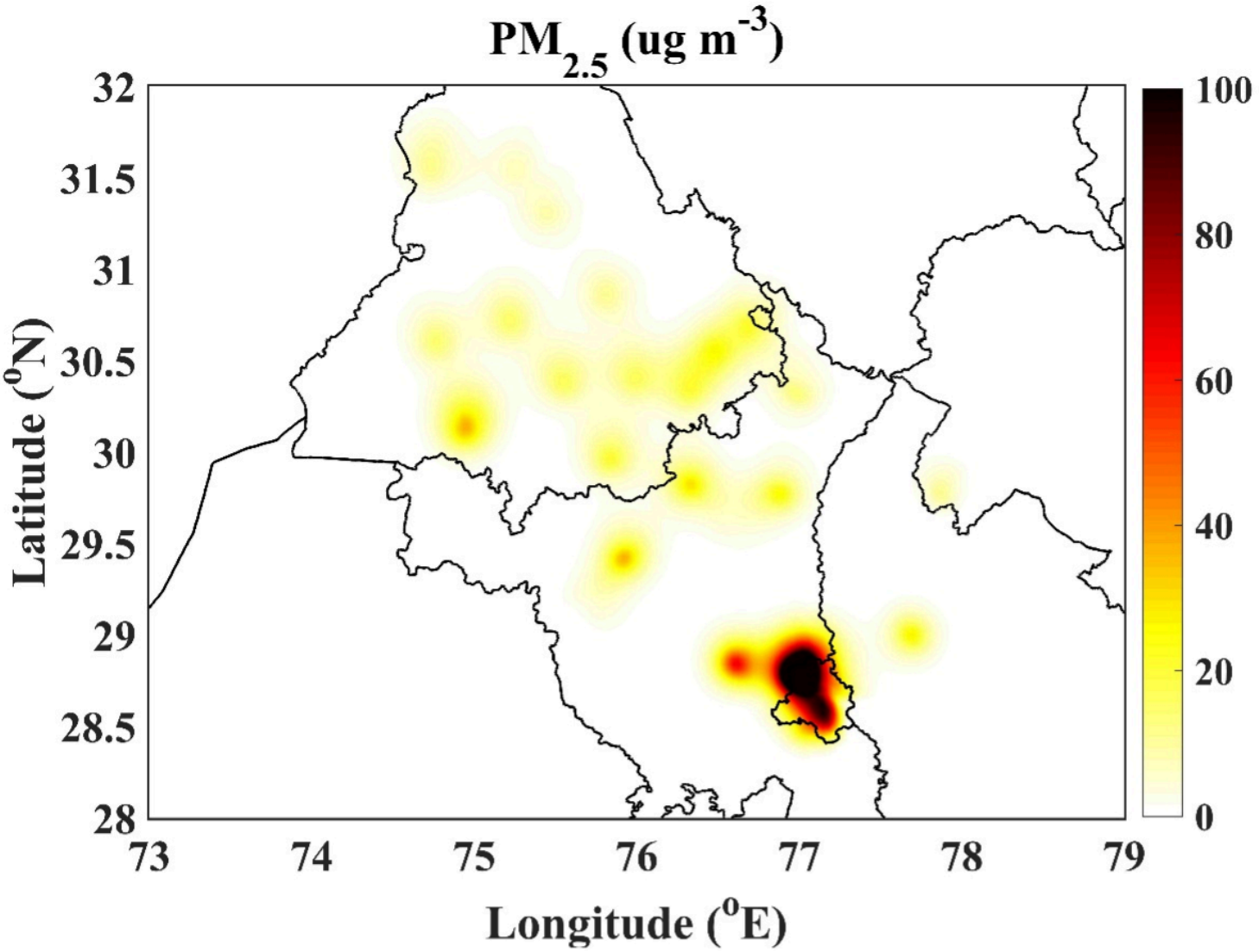


Figure 5

Hourly-averaged surface $PM_{2.5}$ difference (μg m^{-3}) between DA-EXP2 and DA-EXP1 (DA-EXP2 minus DA-EXP1) over the simulation period 10–21 November 2024. Positive values indicate higher $PM_{2.5}$ recovered by DA-EXP2, reflecting the greater observational weight assigned under its smaller fixed observation error.

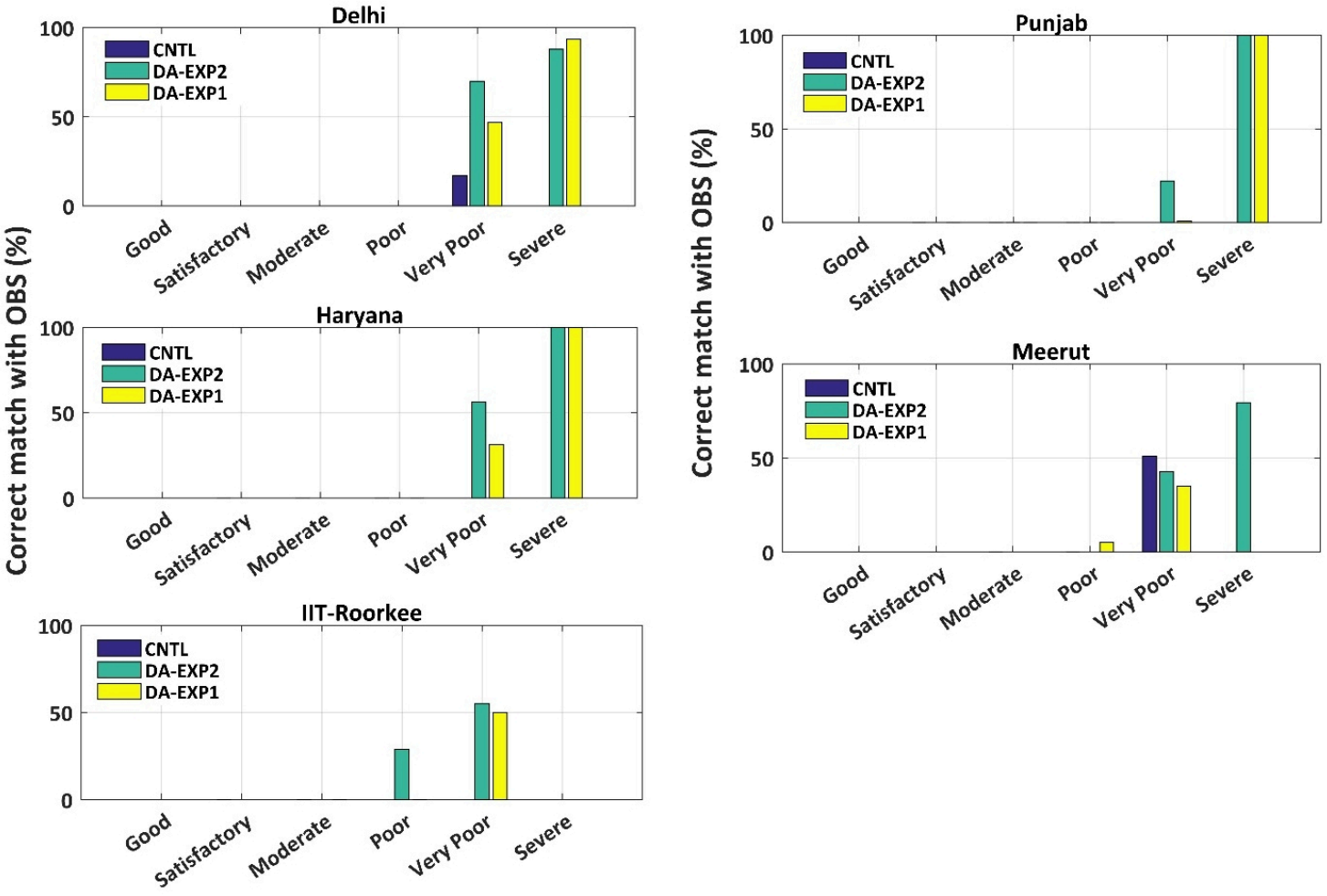


Figure 6

AQI category match percentage (%) for CNTL (blue), DA-EXP2 (teal), and DA-EXP1 (yellow) across five regions: Delhi, Punjab, Haryana, Meerut, and IIT-Roorkee, over the simulation period 10–21 November 2024. For each AQI category — Good, Satisfactory, Moderate, Poor, Very Poor, and Severe — the bars represent the percentage of hours at which the simulated $PM_{2.5}$ falls in the same category as the CUPI-G observation, conditioned on the observation belonging to that category.

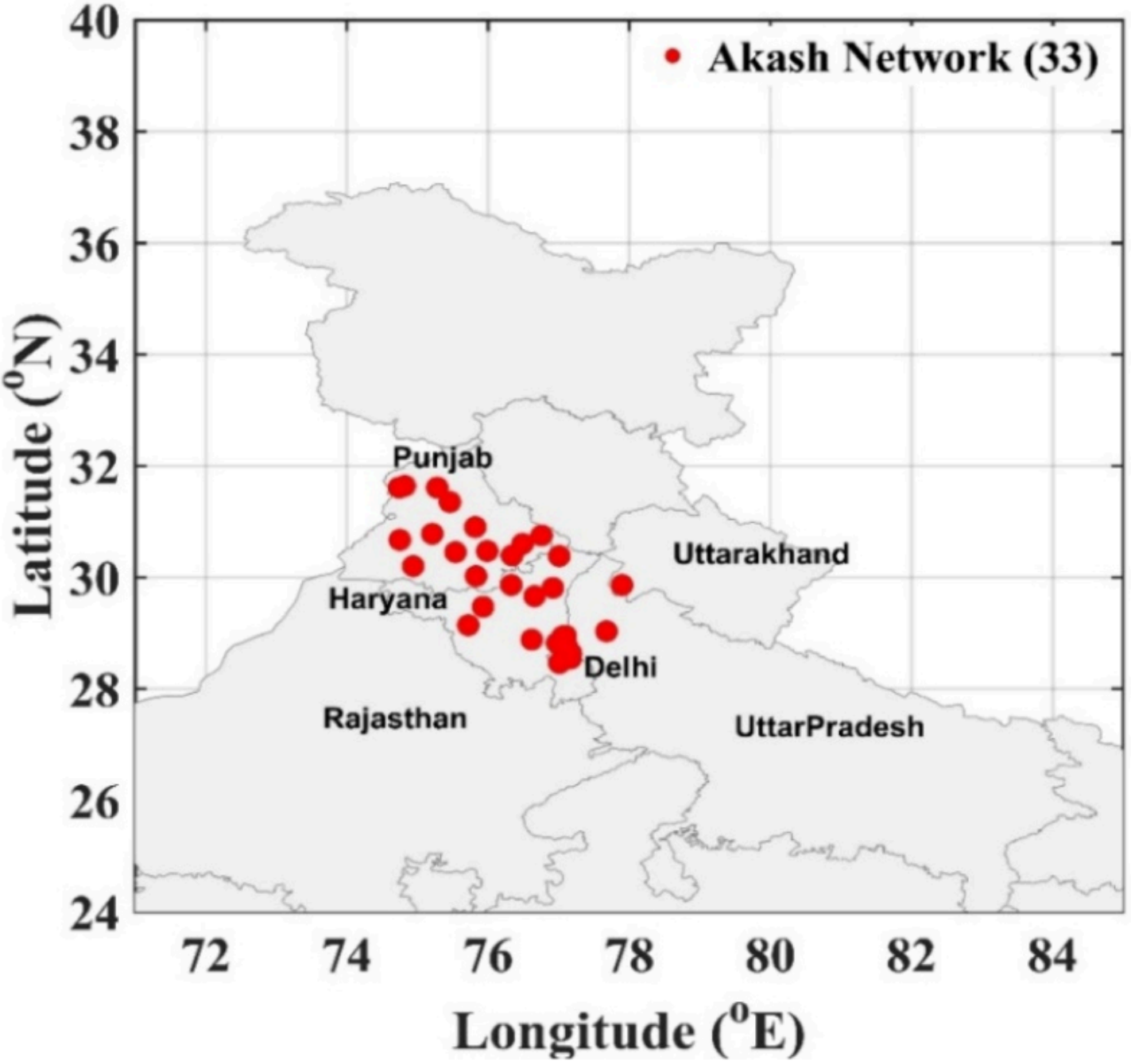


Figure 7

Spatial distribution of the 33 Aakash CUPI-G low-cost sensor sites (red circles) across Punjab, Haryana and the Delhi-NCR during the November 2024 campaign.

Supplementary Files

This is a list of supplementary files associated with this preprint. Click to download.

- supplementary.docx